



ELSEVIER

Contents lists available at ScienceDirect

Annals of Nuclear Energy

journal homepage: www.elsevier.com/locate/anucene

Optimizing variance reduction in Monte Carlo eigenvalue calculations that employ the source iteration approach



Kenneth W. Burn *

ENEA, Via M.M.Sole, 4, 40129 Bologna, Italy

ARTICLE INFO

Article history:

Received 23 September 2013

Received in revised form 11 June 2014

Accepted 17 June 2014

Available online 15 July 2014

This paper is dedicated to the memory of Lodovico Casalini (1955–2010) and of Carlo Artioli (1946–2014).

Keywords:

Monte Carlo

Eigenvalue

Source-iteration method

Variance reduction

Direct statistical approach

ABSTRACT

The question of variance reduction within the source-iteration scheme of a Monte Carlo eigenvalue calculation is tackled. The trade-off point between improving the statistics of a local response whilst simultaneously not damaging excessively the fundamental mode, the source for the calculation of the local response in the next fission cycle, is found. It is realized that applying less normalizations, i.e. employing superhistories, is advantageous. Realistic test problems, both fast and thermal fission, with in- and ex-core local responses, are treated. There is a good agreement between the predicted and actual gain in efficiency. A single comparison with the classic formalism, based purely on ϕ^* , shows large differences.

© 2014 Elsevier Ltd. All rights reserved.

1. Introduction

Variance reduction (VR) methods for fixed source Monte Carlo radiation transport calculations have been extensively developed over the last decades (see for example X-5 Monte Carlo Team, 2005, Vol. I, Ch. 2, pp. 2–134 to 2–163 and Refs. 133–138 therein). They have been extended (Booth, 1992, 2002) to include the behavior of groups of particles, exemplified by pulse-height or coincidence detectors. However to the author's knowledge the improvement and occasional optimization of VR has been confined to fixed source problems (Burn, 2011; Booth, 2012), with the exception of some concepts of global VR (Becker et al., 2007; Wagner et al., 2007; Solomon et al., 2009; Van Wijk et al., 2011), where mention is made of application to reactor cores. (An effort has also been made by Jinaphanh (2012) to employ VR in eigenvalue problems to accelerate convergence to the fundamental mode.) Applied to depletion problems in reactor cores, a global VR approach that aims to keep the statistical error as constant as possible everywhere in the fissile region looks to be based on the logic that less important parts of the core at the beginning of cycle that in an analog Monte Carlo run (understood in this context as one that does not employ VR) have higher statistical errors

associated with their fluxes, later on in the reactor cycle will become more important.

That the application of refined VR has focused on fixed source problems is not surprising: a problem consisting of many orders of magnitude attenuation and a number of source-detector channels solicits a critical employment of the best variance reduction. However deep penetration does not necessarily result from material attenuation, but may also ensue from the geometry – i.e. a spatially limited response, and also from the energy dependence of the response function. (An example was the calculation of the activation rate of ^{94}Zr and ^{96}Zr in a wire inside the core of a WWR-SM research reactor (Burn, 1996). This was actually accomplished by changing the eigenvalue problem to a fixed source one and calculating a single fission generation.)

In the case that the response is outside the core, the usual approach is to decouple the eigenvalue in-core calculation from the ex-core part. This author has always followed the practice of employing the fission sites as the point of coupling of the two parts of the calculation. The advantage is that three of the six phase space variables required to define the fixed source for the second calculation and that govern the direction and energy of the starting neutron have distributions that are known (isotropic and, for example, the Watt fission spectrum). The fission sites are then binned into a number of volumes that cover the whole of the fissile region and starting sites in the second calculation are sampled

* Tel.: +39 0516098417.

E-mail address: kburn@enea.it

from these volumes. It is usually straightforward to define the spatial discretization for the binning (as the distribution of fission sites is relatively smooth). Other workers employ the leakage current from the core. However the author has wondered if such decoupling by one means or another is actually necessary.

Eigenvalue problems are not only confined to reactor cores. Criticality safety of fuel storage also requires an eigenvalue approach. A small neutron detector placed in or near an array of fissile material may be a high attenuation problem due to the size of the detector.

2. Portrayal of the problem

Experience in fixed source calculations has shown that altering the sampling (i.e. splitting and Russian roulette) should be the main workhorse of any VR for general problems. [If in a particular problem biasing is useful (e.g. source biasing, exponential transform) then the alteration of the sampling should include limiting the track's weight, *viz.* the weight window (Booth, 2006).] Thus to calculate one or more localized responses, the track population is altered, sometimes dramatically, from its analog distribution so as to achieve acceptable statistics for those responses.

The source iteration (or power iteration) method is the usual means of solving the eigenvalue problem. Once the fundamental eigenmode has been reached, this method continuously recalculates it by rerunning fission generations (Brown et al., 2009):

$$(L + T - S)\Psi^{(n+1)} = \frac{1}{k_{\text{eff}}^{(n)}} F \Psi^{(n)} \quad (1)$$

where L , T and S are the leakage, collision and in-scatter operators, F is the fission multiplication operator, $\Psi^{(n)}$ is the solution at the n 'th cycle and $k_{\text{eff}}^{(n)}$ is the effective multiplication factor at the n 'th cycle.

In many large loosely-coupled problems (e.g. a PWR core) the Monte Carlo estimate of the fundamental mode fluctuates around the actual solution. In constantly re-estimating the fundamental mode, the source iteration method aims to cover the actual solution.

As the problem is never precisely critical, running a number of fission generations leads to a decay of the neutron population if it is sub-critical or an explosion of the neutron population if it is super-critical. To maintain the neutron population at approximately the same level so as to be able to construct statistics for the responses, the population is normalized after each fission generation (Brown et al., 2009) by the factor M_0/M_1 where:

$$E[M_1] = k_{\text{eff}} M_0 \quad (2)$$

and where M_0 is the number of neutrons starting some cycle and M_1 is the number of fission neutrons produced at the end of that cycle.

[Furthermore, as well as forcing the number of fission neutrons to be (roughly) constant at each generation, it is also normal practice to start fission neutrons in a particular fission generation all with the same weight, even if variance reduction that alters the track's weight is employed in the previous generation. This practice is followed here.]

Such normalization leads to a bias in the responses (Brown et al., 2009; Brissenden and Garlick, 1986). In addition, the estimated errors on the responses are biased due to unaccounted-for correlations (Brissenden and Garlick, 1986). Finally there is the question of how long it takes to reach the fundamental mode and how to judge that it has in fact been reached. These problems can all be, at least partially, resolved, but this does not form part of this work. Suffice to remark here that once the fundamental eigenmode has been reached, allowing an analog simulation of the neutron tracks means that it will be constantly returned to, as in expression (1).

Returning to fixed source deep penetration problems, a detailed mathematical approach called the DSA (Direct Statistical Approach) has been developed that optimizes the VR parameters that govern the sampling (Dubi et al., 1982; Dubi, 1985; Burn, 1992, 1995). The approach has been extended in Burn (1997) to include weight control. Basically it looks for the optimum trade-off between splitting more so as to get more tracks to the detector and splitting less, and with the time thus gained running more independent source particle histories.

The success of the DSA in a wide variety of transport problems (Booth and Burn, 1993; Burn et al., 2005) prompted an attempt to exploit a (somewhat weak) analogy between the fixed source and source-iteration approaches: the above trade-off in fixed source problems (splitting more with less source particle histories/splitting less with more source particle histories) with the trade-off in source-iteration eigenvalue calculations of running more fission generations with a smaller number of fission neutrons per generation/running less fission generations with a greater number of fission neutrons per generation. However this has not as yet yielded results. Instead a more limited goal was set as described in the next paragraph.

This goal was, given a particular size and number of fission generations and given the availability of an acceptable estimate of the fundamental mode, to find the best sampling within each fission generation when it is desired to calculate one or more localized responses as well of course as the usual integral k_{eff} value. In other words the best trade-off was sought between altering the track population by forcing tracks to the vicinity of a localized detector and not letting this damage too much the fundamental mode (which is the source for the next fission generation in which again the localized detector will be estimated, and so on). The approach to achieve this is described in Sections 4 and 5.

3. The DSA with fixed source problems

The DSA applies basic statistical considerations to the VR techniques of surface splitting and Russian roulette (RR). The quality factor q is defined as the product of S^2 , the population second moment of some detector response whose average value is given by the first moment, D , and τ , the average time per source particle history:

$$q = S^2 \cdot \tau \quad (3)$$

In Dubi et al. (1982) it is shown that $1/q$ is some measure of the statistical efficiency of the Monte Carlo calculation: the population variance V is:

$$V = S^2 - D^2 \quad (4)$$

The square of the first moment can normally be neglected (Dubi et al., 1982). Then if the number of histories in the sample is N ,

$$V = V_S \cdot N \quad (5)$$

$$\tau = \frac{T_S}{N} \quad (6)$$

where V_S is the sample variance and T_S is the sample time.

If in defining q we employ S^2/D^2 , instead of S^2 , then $1/q$ is analogous to the well-known figure-of-merit (X-5 Monte Carlo Team, 2005, Vol. I, Ch. 1, p. 1–7), defined as the inverse of the product of the square of the relative error (fsd) and the sample time:

$$\text{fom} = \frac{1}{\text{fsd}^2 \cdot T_S} \quad (7)$$

In this work a number of responses D_i , $i = 1, M$ will be considered simultaneously. This leads us to consider a compound quality

factor, q_c , defined as the product of a compound second moment, S_c^2 , and average time τ per source particle history [see expression (1) in Burn (2011)]:

$$q_c = \sum_{i=1}^M \frac{S_i^2}{D_i^2} \cdot \tau \quad (8)$$

and $1/q_c$ is analogous to a compound figure-of-merit, fom_c , defined as:

$$fom_c = \left[\sum_{i=1}^M (\text{fsd}_i)^2 \cdot T_S \right]^{-1} \quad (9)$$

Maximizing $1/q_c$ is equivalent to maximizing fom_c if the variance can be approximated by the second moment.

Two DSA versions exist: a weight-independent (Burn, 1995) and a weight-dependent (Burn, 1997) model. Both models have been extensively tested for fixed source problems and have been converted to run with the source-iteration scheme in eigenvalue problems, as discussed in Sections 4 and 5. However the sample problems in Section 6 all employed the weight-independent model, which will therefore be the only model referred to here.

3.1. The weight-independent splitting/RR model (Burn, 1995)

Splitting/RR is executed at boundaries between closed volumes or cells, J and K (see Fig. 1) in phase space (currently space and energy) according to the ratios of parameters ("importances") assigned to each cell. The second moment S^2 is given by the sum of three terms: Δ^s , Δ^v and Γ . The first two terms take account of the correlations between detector scores from tracks coming from the same bifurcation (i.e. track branching: a track dividing into two or more progeny). Such branching may be artificial (i.e. for variance reduction) or natural [e.g. fission, (n,xn)]. Δ^s represents bifurcations at surfaces (i.e. surface splitting). Δ^v represents bifurcations in volumes. The third term, Γ , results from the individual direct detector scores.

$$\Delta^s = \sum_{\text{source cells } j_0} F(j_0) \sum_{\text{each boundary between cells } J/K} \text{coef}_d(j_0; J/K) \cdot \frac{\text{int}[G(J/K)]}{F(K) \cdot G(J/K)} \cdot \{2 \cdot G(J/K) - \text{int}[G(J/K)] - 1\} \quad (10)$$

$$\Delta^v = \sum_{\text{source cells } j_0} F(j_0) \sum_{\text{each cell } J} \text{coef}_d(j_0; J) \cdot \frac{1}{F(J)} \quad (11)$$

$$\Gamma = \sum_{\text{source cells } j_0} F(j_0) \left\{ \text{coef}_g(j_0; j_0) \cdot \frac{1}{F(j_0)} + \sum_{\text{each cell } K} \text{coef}_g(j_0; K) \cdot \frac{1}{F(K)} \right\} \quad (12)$$

$$S^2 = \Delta^s + \Delta^v + \Gamma \quad (13)$$

Expressions (10)–(12) are equivalent to expressions (27), (30) and (36) respectively in Burn (1995), but with a less cumbersome

notation. In all three expressions, the outer sum over j_0 represents the sum over source cells. In expression (10) each term within the inner summation represents the contribution from splittings at the boundary between cells J and K (see Fig. 1) with importances $F(J)$ and $F(K)$ respectively [and $G(J/K) = F(K)/F(J)$]. These terms are then summed over all cell boundaries J/K . In expression (11) each term within the inner summation represents the contribution from all types of volumetric bifurcations within each cell J . These terms are then summed over all cells J . In expression (12) each term within the inner summation represents the contribution from detector scores from each cell K , $K \neq j_0$. These terms are then summed over all cells K . The first term within the outer summation represents the contribution from detector scores from the source cell j_0 .

The $\text{coef}_x(\dots)$ variables are problem-dependent coefficients whose values must be estimated. " $\text{coef}_d(j_0; J/K)$ " in expression (10) involves the product of the square of the track's weight as it crosses a cell boundary and the square of the adjoint flux at the crossing point [see expressions (25) and (26) in Burn (1995)]. " $\text{coef}_d(j_0; J)$ " in expression (11) involves the product of the square of the track's weight as it experiences a bifurcation within a cell and the product of the expected detector contributions of each pair of branches at the bifurcation point [see expressions (23), (28) and (29) in Burn (1995)]. " $\text{coef}_g(j_0; j_0)$ " and " $\text{coef}_g(j_0; K)$ " in expression (12) involve the square of a track's detector score [see expressions (32), (33) and (35) in Burn (1995)].

The time τ is given as:

$$\tau = \sum_{\text{source cells } j_0} F(j_0) \left\{ \text{coef}_t(j_0; j_0) \cdot F(j_0) + \sum_{\text{each cell } K} \text{coef}_t(j_0; K) \cdot F(K) \right\} \quad (14)$$

Expression (14) is equivalent to expression (43) of Burn (1995), but again with slightly less cumbersome notation. Each term within the inner summation represents the CPU time spent by tracks within a cell K . These terms are summed over all cells K , $K \neq j_0$. The first term within the outer summation brackets represents the CPU time spent by tracks within each source cell j_0 . The problem-dependent coefficients which must be estimated: " $\text{coef}_t(j_0; j_0)$ " and " $\text{coef}_t(j_0; K)$ " consist of linear or first moment-like quantities that measure the average calculational time spent on tracking in each cell [see expressions (39), (40) and (42) of Burn (1995)].

3.2. Realization in fixed source problems

As illustrated in the previous section, S^2 and τ are described in terms of coefficients and a splitting/RR parameter dependence. The coefficients are generated using Monte Carlo. Once the second moment and time function coefficients are generated, a separate minimization code is employed to find the set of VR parameters that minimizes q . [This code (Burn, 1992) has been written around an IMSL routine.] As with any approach that employs Monte Carlo to generate information which is then used by Monte Carlo to improve the calculation, a number of iterations may be required. The procedure is given as follows:

- Guess some VR parameters
- Entry point
- Estimate the second moment and time function coefficients with the current VR parameters
- Plug the second moment and time function coefficients into the functions and extract the VR parameters that minimize q
- With these VR parameters either go back to the entry point or exit

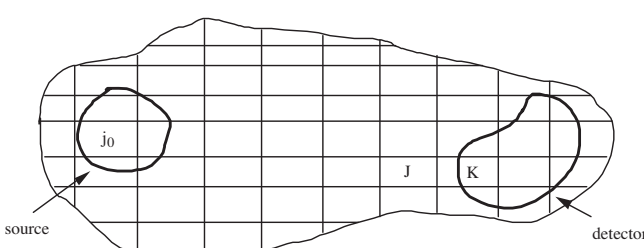


Fig. 1. General cell configuration.

The first set of guessed VR parameters may themselves require some kind of iterative procedure to generate – in fixed source deep penetration problems a certain experience is also helpful.

4. Description of the new approach to eigenvalue problems

Some years ago a multi-response capability (Burn and Nava, 1997; Burn et al., 2000; Burn and Gualdrini, 2002; Burn, 2011) was included in the DSA for fixed source problems. In contradistinction to the previously mentioned effort aimed at global VR (Becker et al., 2007; Wagner et al., 2007; Solomon et al., 2009; Van Wijk et al., 2011), this capability was aimed at a limited number [“M” in Eqs. (8) and (9)] of responses, and firstly at a limited part of phase space. The number of responses as well as their extension in phase space was increased, so now some hundreds of responses can be treated. This number though remains limited as again in contrast to the global effort, the theory is not linear (viz. the presence of the square of the adjoint flux in the coefficients as mentioned in Section 3.1) so each response must remain distinct (Burn, 2011) and provide a distinct adjoint flux.

The DSA multi-response capability looked an appropriate tool to alter the sampling in a source-iteration eigenvalue scheme, for some local response(s) and for the fundamental mode simultaneously. Note that the fundamental mode is a distribution rather than a single response. To sample a distribution, it has to be divided into a number of parts (in a similar way to the division of an energy spectrum into a number of energy groups). As the fundamental mode is relatively smooth, the number of parts did not have to be too large – typically a division of the fissile region into 10–20 parts was sufficient. The tallies that mock up the fundamental mode will be referred to here as “global tallies” to distinguish them from the above local ones.

In the absence of any VR, as discussed in Section 2 the distribution of fission sites at the end of each fission generation will tend to return to the fundamental mode distribution [see expression (1)] [with stochastic variations around the mean, or actual, distribution (Brissenden and Garlick, 1986)]. Introducing population distortion, or skewing, to improve the statistics of the local detector(s), means that even if the fundamental mode is mocked-up by a number of responses which are simultaneously included in the optimization, the variance around the mean of the fundamental mode distribution after each fission generation will probably increase. As the fundamental mode distribution is the source distribution for the next round of sampling of the local response/fundamental mode, and so on, a major concern was that the fundamental mode should not be permanently distorted. In other words the concern was that the skewing of the track population to sample the local detector(s) within a fission generation might be such that the weight-equalization at the normalization step, discussed in Section 2, distorted the fundamental mode. The source for the next generation would then be wrong.

Although the inclusion of a number of responses to mock-up the fundamental mode distribution as discussed above is intended to solve this problem, it looked beneficial to recalculate the fundamental mode a number of times without equalizing the weights and thus postpone the normalization point, i.e. run superhistories (Brissenden and Garlick, 1986). Then if the fundamental mode components were also responses-of-interest as well as the local response(s) at every fission generation within the superhistory, it was thought that this would constrain the variation of the fission rate around its real value after each fission generation and hopefully allow a suitable trade-off with the quality of the local response to be achieved, limiting the distortion of the fundamental mode to a statistical fluctuation. This option was the one adopted.

The option of not running superhistories but including the local response and the fundamental mode (binned into a number of responses) in a single fission generation is illustrated in Fig. 2. The adopted option of running superhistories is illustrated in Fig. 3 (with the example of one superhistory consisting of four fission generations). In these figures the dashed lines represent the interface between fission generations and a subdivision of the fundamental mode is represented beside or below the dashed lines (as a reminder that the optimization also includes the responses that make up the fundamental mode). However for illustrative purposes, only the localized response is assumed to be present (represented as the small square), that then tends to increase the concentration of the tracks in its vicinity.

A number of further clarifications may be made:

Following the usual source-iteration logic, with or without superhistories, it is assumed that each normalization generation starts off with its own independent source. As mentioned, the starting tracks in this source must have equal weight, thus any population skewing due to sampling that forces tracks to the local response should be negated at the point of normalization. Instead for fission sources within a superhistory, the population variation due to the sampling is maintained. Although the track population is skewed, when the track weights are taken into account, the expected fission source distribution is unaltered. Thus the expected value of the local response in the next fission generation within the superhistory is unaltered, and so on.

Another motive for adopting superhistories was to allow more fission generations for the neutron tracks to be forced to the vicinity of the local detector, i.e. allow more “space” to get the tracks to the detector. Then as mentioned previously, at the end of the superhistory low weight tracks in the vicinity of the local detector will likely be rouleotted.

Within each superhistory, as well as the correlations between progeny from the same splitting event (such splitting forcing tracks toward one or other of the multiple responses), there will also be correlations between the local detector scores separated by one, or more, within-superhistory fissions. Furthermore there will be correlations between the scores of the responses that make up the fundamental mode and the scores of the fission neutrons in future fission generations (up to the end of the superhistory), both those contributing to the fundamental mode and those contributing to the local detector(s). All these correlations are taken into account with the DSA (Burn, 1995).

5. Implementation of the new approach in eigenvalue problems

The DSA algorithms have been programmed in “patch” form using the code MCNP (X-5 Monte Carlo Team, 2005) as vehicle.

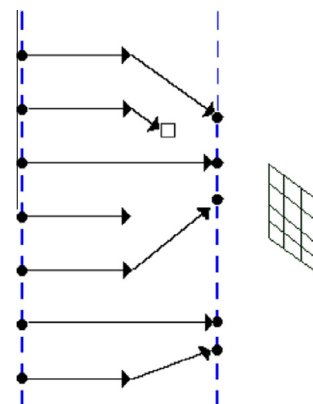


Fig. 2. Illustration of a single fission generation with a localized response.

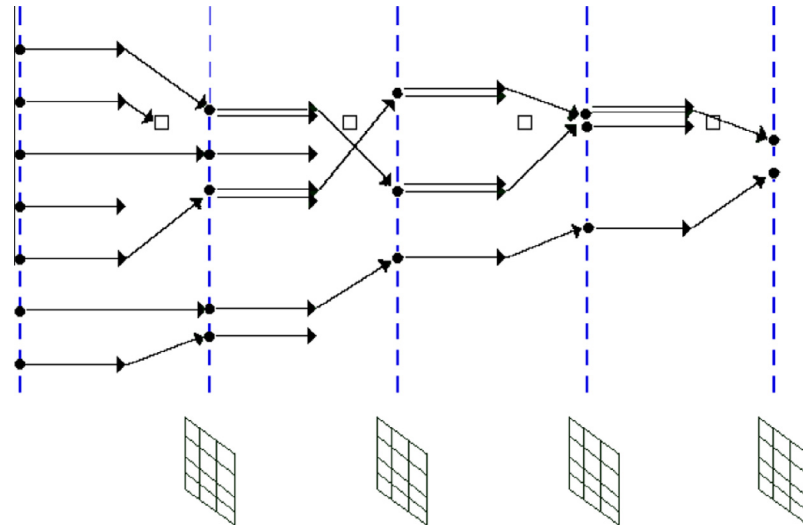


Fig. 3. Illustration of a superhistory containing four fission generations with a localized response.

In principle, and appropriately modified, the patch could be applied to any standard Monte Carlo code. Before the present work, the last major update was in 2010–2011 to parallelize the patch with MPI to be compatible with MCNP version 5–1.4.

5.1. Differences between normal Monte Carlo and the DSA

In normal Monte Carlo the amount of output information (i.e. results and tallies) is relatively small and in any case fixed whilst in the DSA the amount is much larger and varies, increasing with the number of histories run. This is due to the employment of the “enhanced point-surface (eps) approximation”. This approximation is described in Sections IV.A and IV.B of Burn (1997) for crossings of boundaries between space/energy cells (where splitting or Russian roulette is applied) and bifurcations at collision points within volumes [e.g. fission, (n, xn), etc.], respectively. This approximation was in fact present in previous weight-independent DSA versions.

As discussed in Section 3, to estimate the second moment at boundary crossings, the square of the adjoint flux is required. To correctly estimate this square (a) at least two progeny are required and (b) to provide a non-zero estimate at each boundary crossing, at least two progeny must score. The condition (a) can be satisfied by altering the normal splitting/RR game (Burn, 1997, p. 152, col. 1), although when there is low splitting or Russian roulette the altered game should be noisier than the normal one. It is straightforward to see that condition (b) produces extremely noisy results. An obvious work-around is to consider arriving progenitors that have similar phase space characteristics as identical, and similarly, to consider starting progeny from bifurcations of these progenitors as identical. Bifurcations at collision points within volumes exhibit analogous numerical problems: at least two branches must score to provide a non-zero estimate of the second moment (Burn, 1997, p. 153, col. 2). For these bifurcations a similar work-around is suggested. Thus a binning of the phase space variables at surface crossing points and at points in volumes where bifurcations occur, is made to calculate the second moment. Such binning is made in energy, in space (to subdivide the crossing point between two spatial cells) and again in space so as to discriminate the angle of the boundary crossing – by logging the point of the next collision of the progeny. (It should also be borne in mind that such binning must be made for each response.) This is the eps approximation.

In shielding problems it has been found that this binning must be sufficiently fine – of course the finer the binning, the better the

second moment. The downside with a fine binning is the size of the array required to approximate the second moment. In fact the array is too large to be dimensioned *a priori* but instead needs to be dynamically allocated, with pointers in a hierarchical structure.

There are some consequences of all this:

- During the track generation much time is spent on finding where in the hierarchy the new data must be inserted and, if a new bin is to be created, making space for the bin at the appropriate position.
- In the case of parallel architecture, after the track generation has finished combining the arrays generated on the different CPU's into a single array is laborious.
- The data increases with the number of histories as more bin combinations are discovered. However in real problems the saturation point is never reached.

These various issues have been resolved but improvements should still be made. The more responses, and the more response contributions that there are, the greater the number of bin combinations that are generated. In eigenvalue problems there tend to be many more response contributions compared with deep penetration fixed source problems. As a consequence the question of data generation and handling is critical.

5.2. Steps taken

The first step was to implement a superhistory algorithm in MCNP5. The number of fission generations per superhistory was allowed to vary as an input quantity. The option was introduced to adjust the v value to ensure a reasonable supply of children at each normalization (Brissenden and Garlick, 1986) for the case that k_{eff} differs appreciably from unity and there are a sufficiently large number of fission generations per superhistory.

Secondly the DSA patch including parallelism, as outlined above, was modified to be compatible with the logic of tally scoring and source normalization under the source-iteration scheme and then integrated with the superhistory patch.

Finally some input and output quantities were differentiated according to the fission generation:

- the responses were subdivided according to the fission generation (or group of fission generations);

- similarly the VR parameters [in the DSA, 2-dimensional energy/space cell importances (Booth and Burn, 1993) or weight lines (Burn, 1997)] were differentiated according to the fission generation (or group of fission generations).

5.3. Realization in eigenvalue problems

As for fixed source Monte Carlo, an iterative procedure is employed to arrive at the optimum VR parameters as described in Section 3.2. An important difference from fixed source problems is that the responses constituting the fundamental mode can be, and are probably best, estimated by analog Monte Carlo (i.e. unity importances). However this may not be sufficient to generate information for the local response(s).

In Section 6, for the sample problems that contain an in-core local response, in some cases unity guessed importances were sufficient. In others, the problem was solved in two steps: the first step with unity guessed importances but with a larger local detector; the second step employing the VR parameters issuing from the first step and the correct size local detector. Instead for the sample problem that contains an ex-core local response, the approach is similar to fixed sources, with the proviso that analog, or nearly analog, VR is carried out as the first guess in the fissile region. In fact for the ex-core problem, the starting VR parameters that were the first guess were based on those from a similar fixed source problem that had been previously treated.

In the sample problems in which the importances varied according to the fission generation, an iterative procedure was followed as described in Section 3.2, with no VR dependence on the fission generation in the first iterations, followed by a VR dependence on the fission generation in later iterations.

6. Test problems

In all the test problems, the asymptotic phase was assumed to have been reached, i.e. the memory of the guessed set of starting fission sites was lost. Notwithstanding, as three of the four problems were loosely coupled, the deviations of the fission sites at each fission generation from the fundamental mode in the asymptotic phase were substantial and in particular involved similar-sign deviations over relatively large volumes due to apparent collective behavior (manifesting itself in a somewhat analogous fashion to “sloshing” in CFD).

The first sample problem, in Section 6.1, was used to test the basic operation of the DSA algorithm and to investigate the three options available: (1) changing the length (and number) of the superhistories; (2) varying which fission generations to tally in; (3) allowing the VR to vary, or not, according to the fission generation. Once these issues were resolved, the solutions found were employed in problems 2, 3 and 4 in Sections 6.2, 6.3 and 6.4.

Capture was treated explicitly (i.e. *not* survival with a weight reduction according to the absorption probability) in all the sample problems.

Terminology: we use the word “importances” for the values assigned to each phase space cell that govern the amount of splitting/RR (Burn, 1990). This is not to be confused with the “importance” or adjoint flux (ϕ^*) which is usually referred to here as the expected future tally contribution. “Importances” that are generated using the adjoint flux only are referred to as “classic importances”.

6.1. PWR 2-D

This problem is based on the UAM LWR NEA Benchmark (Ivanov et al., 2011). Slight differences are the core assembly configuration,

fuel composition and the reflector configuration. The reflector is steel but rather than occupying an assembly position immediately outside the ring of peripheral fuel assemblies [Fig. 35 of Ivanov et al. (2011)], has an inner surface that follows the outer surface of the peripheral fuel assemblies and a cylindrical outer surface (Figs. 4 and 5).

This problem was actually originally employed to study the phenomenon of flux tilt (Burn et al., 2012) and for simplicity is 2-dimensional. To achieve the tilt, the water density was increased slightly (1.5%) in the outer assemblies of the SE core quadrant and decreased by the same amount in the outer assemblies of the opposite NW quadrant (Fig. 4). The power density was then studied throughout each of the 4 core quadrants (Fig. 5).

The steel reflector tends to accentuate perturbations in the outer part of the core and it turns out that the problem is numerically quite unstable. As a consequence, even when the transient phase has been passed and the asymptotic phase (i.e. the fundamental mode) has in principle been reached, there is still an appreciable fluctuation from fission generation to fission generation, even in integral quantities such as the quadrant power. This, notwithstanding the fact that the number of fission neutrons per generation was quite high –500,000 or 1,000,000. Hence, as already discussed, the real fundamental mode is covered by the simulated one only because of its repeated estimation within the source-iteration method. Thus within the generational logic of the source-iteration scheme, the variance may be subdivided into a part due to the stochastic transport of neutrons from a given simulated set of fission sites at the beginning of some generation following the transient phase (until the next generation) and a part due to the fluctuation between sets of starting fission sites, from generation to generation.

6.1.1. Varying the length and number of superhistories and the fission generations used for tallying

Firstly some combinations of the first two options (length and number of superhistories, which fission generations to tally in) were examined, keeping the VR parameters independent of the generations. As discussed in Section 4, the greater the length of a superhistory, the more “space” is available to get tracks to the local detector. (Instead the downside of longer superhistories is a more difficult population control when k_{eff} differs appreciably from unity (Brissenden and Garlick, 1986), and a higher variance.) Furthermore whilst as stated in Section 4 it looks desirable to tally the fundamental mode components as well as the local response(s) at every fission generation within the superhistory (disregarding

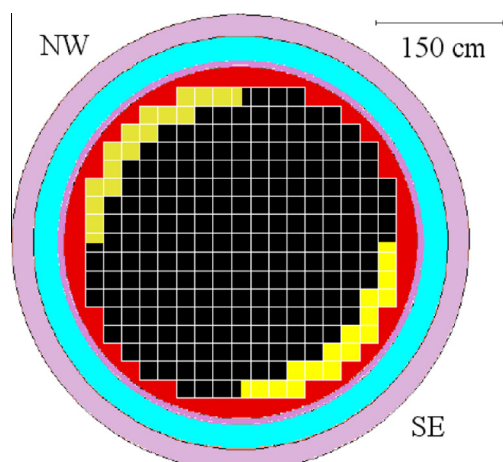


Fig. 4. PWR 2-D problem showing assemblies where the water density has been increased and decreased.

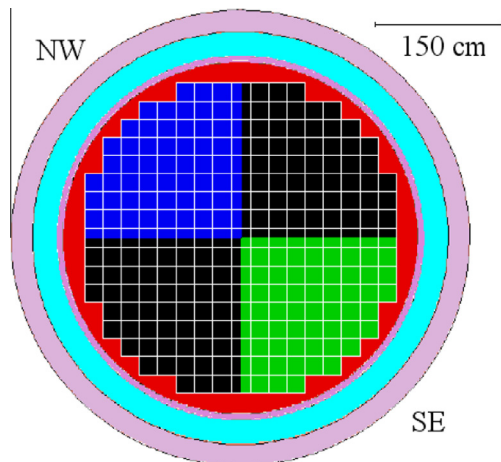


Fig. 5. PWR 2-D problem showing assemblies in each quadrant where the power density was tallied.

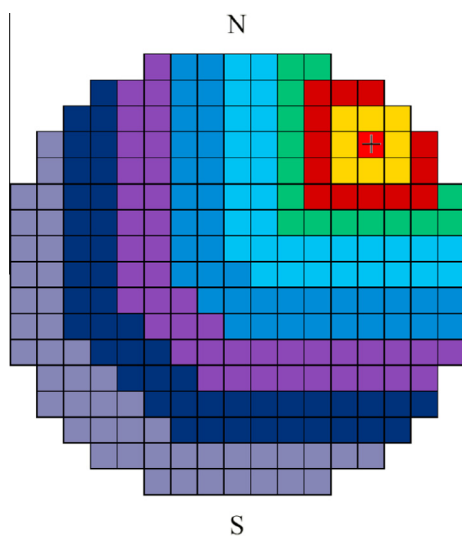


Fig. 6. PWR 2-D problem showing position of assembly with local detector and core subdivision for VR.

other issues, the statistics should be better), it was of interest to examine some cases where this was not done.

Bearing in mind the discussion above, there were four “global” responses to mock-up the fundamental mode – the fission heating rates in each of the four quadrants (see Fig. 5). The local response was chosen as the fission heating rate in a single pin – there are 17^2 pins in each assembly (24 of which are guide tubes) and 241 assemblies in the fissile region (Ivanov et al., 2011).

The assembly chosen for the local response was near the periphery of the fissile region – see Fig. 6 – and the pin was the central fuel pin of that assembly as shown in Fig. 7. Also shown in Fig. 6 is the assembly subdivision for VR: a total of 9 zones: the assembly containing the local response (+); each of the three surrounding rings of assemblies; then five rings of assemblies, each ring consisting of 2 assembly widths. Further subdivisions of the geometry were made outside the fissile region, making a total of 29 spatial cells. 6 energy groups were employed for VR with limits: 500 keV, 50 keV, 5 keV, 100 eV and 1 eV.

Figs. 8 and 9 show the eight cases that were firstly examined. Each case employed a superhistory size of 1 M fission neutrons, apart from case G (500,000 fission neutrons).

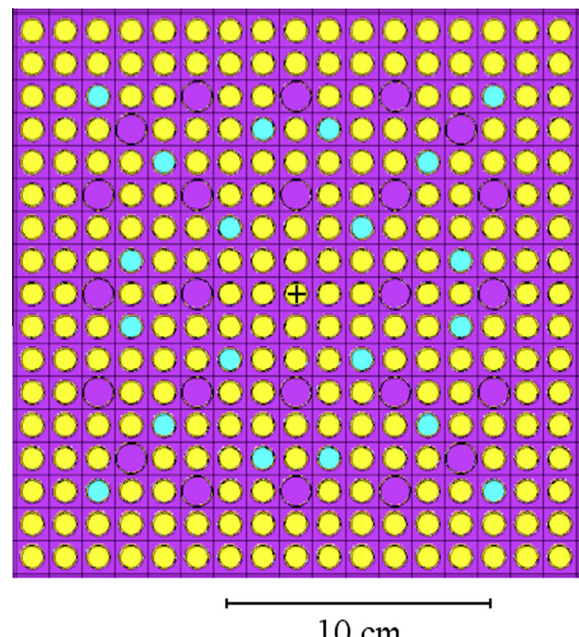


Fig. 7. PWR 2-D problem showing central pin of the assembly (marked with a cross) employed as the local detector.

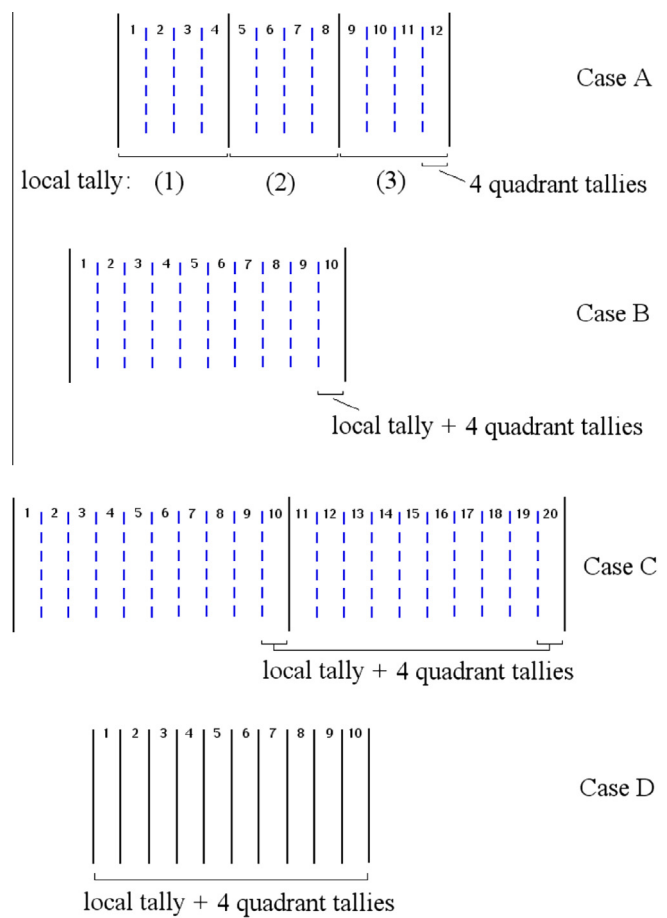


Fig. 8. PWR 2-D problem: schematic of cases A, B, C and D (superhistories/fission generations/tallies).

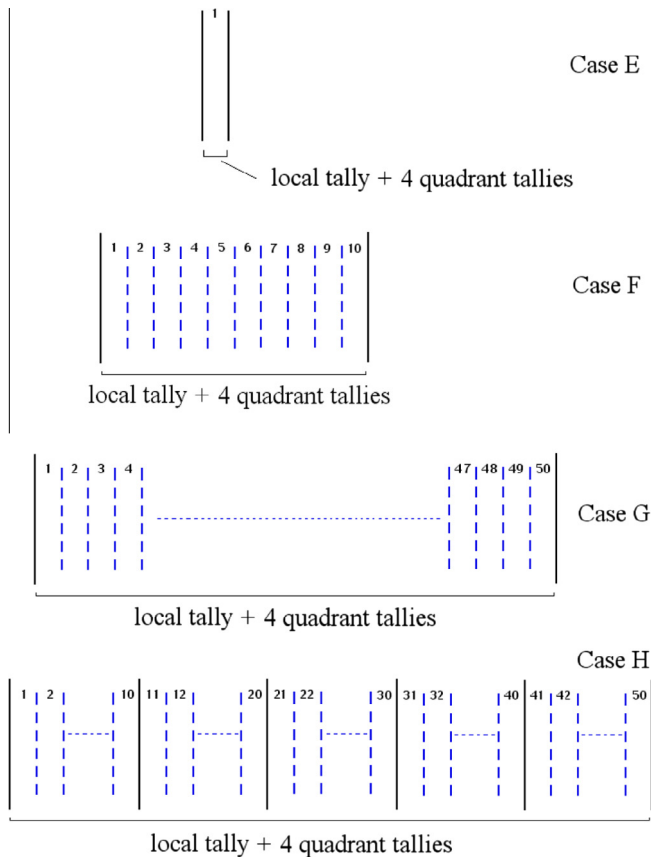


Fig. 9. PWR 2-D problem: schematic of cases E, F, G and H (superhistories/fission generations/tallies).

- Case A has 3 superhistories, each containing 4 fission generations, and 3 independent but identical local responses, for all 4 fission generations in each superhistory. The global, quadrant, tallies are for the last fission generation of the last superhistory.
- Case B has a single superhistory containing 10 fission generations. Both the local and global tallies are for the 10th fission generation.
- Case C is like B but with 2 superhistories and the tallies are the combined signals from the last fission generation of each superhistory.
- Case D instead has 10 superhistories, each containing a single fission generation. The tallies combine the signals from all the generations.
- Cases E, F and G all have a single superhistory containing respectively 1, 10 and 50 fission generations. The tallies combine the signals from all the fission generations.
- Case H, like G, has a total of 50 fission generations, but they form 5 superhistories. Again the tallies combine the signals from all the fission generations.

As the configuration is only slightly supercritical, the ν value was not altered, even for the case of 50 fission generations in 1 superhistory. For each case an analog run (in this context, a run employing unity importances – there may still be some non-analog features in the data) was made to generate the second moment and time function coefficients, required in the DSA formalism as discussed in Sections 3 and 5. The VR parameters were then found that minimized q_c (Section 3) and a run was made employing these “optimum” parameters. For cases A–G, Table 1 shows the direct

estimates of $1/q_c$ for the analog run and for the “optimum” run and their ratio, together with the DSA function value and the direct estimate of the compound second moment S_c^2 (Section 3) for the “optimum” run and their ratio. [It is more interesting to compare S_c^2 for the “optimum” rather than the analog run as for the analog run the Δ^S terms (see Eq. (10)) are zero.]

In Table 1 we see in the first three columns a relatively good agreement between the direct estimate of the second moment and its function value. [We remind ourselves that the function value employs the enhanced point-surface approximation. Notwithstanding the relatively fine binning employed with this approximation (see Section 5.1), in deep penetration fixed source problems the second moment function value may be up to a factor of 3 different from the direct estimate. Nevertheless such a function still gives rise to a reasonable optimum – see the various sample problems treated (Booth and Burn, 1993; Burn, 1996; Burn and Nava, 1997; Burn et al., 2000; Burn and Gualdrini, 2002; Burn et al., 2005).] Of the two cases, A and E, that show some difference between the function value and the direct estimate of S_c^2 (a factor of 2 or so), in case E this is assumed to be due to too small a sample (a single fission generation only – at least 10 times less fissions than the other cases). Instead case A breaks certain assumptions intrinsic to the model. An assumption of the Monte Carlo modeling is that sampling from more starting sets is equivalent to resampling from the same source. However as discussed at the beginning of Section 6.1, even with 1 M starting neutrons there is an appreciable fluctuation in the starting set from generation to generation. Thus in case A different tallies are subject to different sources.

As far as the $1/q_c$ values in Table 1 are concerned, as already stated the more fission generations that are tallied, the better will be the statistics. We see this effect in the low $1/q_c$ values for cases B and C. (Not apparent from these results is any possible distortion to the fundamental mode induced by not tallying the global and local responses in all the fission generations, mentioned in Section 4. It will simply be assumed that it is better to tally in all the generations.) Also the more fission generations there are, the better the real source is sampled. Furthermore as discussed in Brissenden and Garlick (1986) and elsewhere, the sources in adjacent fission generations are correlated whilst in Table 1 both the directly estimated and the function values assume that the source histories are independent. [It has been found empirically (Brissenden and Garlick, 1986) that a superhistory length of 10 fission generations reduces the source correlation to reasonable values for most problems, including loosely coupled ones.] Therefore we suspect the results for case D for reasons of correlation and also suspect the tendency to reduce the $1/q_c$ value in cases E → F → G because of the ever increasing number of fission generations. Thus case D is not necessarily the best case and G is not necessarily the worst.

Cases D, E, F and G were further examined by running 20 independent calculations (each starting with a different random number seed) for the analog and for the “optimum” importances. Looking at the statistics between the 20 sets of results gives us a compound figure-of-merit (fom_c) (Section 3) that can be compared with the $1/q_c$ values generated in a single run. The results are shown in Table 2. The subscript “fcn” denotes a $1/q_c$ value using the DSA second moment and time functions. The subscript “est” denotes a direct estimate. (The subscript “opt.anal” denotes the functional $1/q_c$ value at the optimum importances of each case with the functions having been generated with the analog importances.)

In Table 2 we see a reasonably good agreement between $1/q_c$ and fom_c apart from case D with optimum importances. Presumably this is due to the correlations between fission generations which result in a real standard deviation that is much higher than the calculated one that assumes no correlations. Instead for cases E, F and G the fom_c

Table 1

Comparison of direct estimates and function values of S_c^2 and of direct estimates of $1/q_c$ for cases A–G of PWR 2-D problem.

Case	S_c^2 opt Direct estimate	S_c^2 opt Function value	S_c^2 (ratio)	$1/q_c$ anal Direct estimate	$1/q_c$ opt Direct estimate	$1/q_c$ (ratio)
A	9.91E+2	4.68E+2	0.472	0.152	2.88	19.0
B	1.19E+3	1.23E+3	1.04	0.0469	0.905	19.3
C	1.01E+3	1.06E+3	1.05	0.0372	0.961	25.8
D	8.62E+2	6.82E+2	0.791	0.404	19.3	47.8
E	1.10E+3	6.35E+2	0.575	0.527	13.4	25.5
F	3.40E+2	3.06E+2	0.899	0.374	2.83	7.57
G	5.59E+2	6.73E+2	1.20	0.189	0.334	2.08

Table 2

Comparison of $1/q_c$ and fom_c for cases D–G of PWR 2-D problem.

Case	Analog				Opt. importances			fom_c opt/ fom_c anal
	$1/q_c$ fcn	$1/q_c$ est	fom_c	$1/q_c$ opt.anal	$1/q_c$ fcn	$1/q_c$ est	fom_c	
D	0.441	0.404	0.746	28.8	24.4	19.3	2.50	3.35
E	0.544	0.527	0.672	41.8	23.3	13.4	24.1	35.9
F	0.361	0.374	0.552	4.02	3.16	2.83	3.68	6.67
G	0.160	0.189	0.210	0.280	0.277	0.334	0.448	2.13

values are reasonably near both the function values and direct estimates of $1/q_c$. Case E looks the best one but of course it is just a single fission generation. Introducing more fission generations ($1 \rightarrow 10 \rightarrow 50$) and also without further source renormalization in-between will introduce more variance as we can see in Table 2.

Case H runs the same number of fission generations as case G but normalizes every 10 generations, like case F. We see in Table 3 that the analog run for case H gives results that are similar to those of case F and not to those of case G. This suggests that the degradation in fom_c in Table 2, cases F → G is due to the intrinsic variance within the superhistory (due to the variable length) and not due to the greater total number of fission generations.

To continue the comparison between cases E, F and G, cases E and F were continued for a further 49 and 4 superhistories respectively. At this point the three cases had an identical number of fission generations. For all three cases, the optimization was run and fom_c 's were generated from 20 independent calculations with the respective optimum importances. The results are shown in Table 4 where a comparison is also made with the results in Table 2 for the optimum fom_c 's from a single superhistory. There looks as if there might be a small advantage in a superhistory consisting of 10 fission generations.

The actual values of the optimum importances will be considered in detail later. Now we just observe that for the spatial cell containing the local response (see Figs. 6 and 7), when the importance in the highest energy group (>500 keV) was unity, the importance in the thermal group (<1 eV) was 228, 114 and 24 for cases E, F and G respectively. We note a very high splitting in case E into the thermal group, that decreases the more fission generations there are in the superhistory. This seems reasonable as, with the case of more than one fission generation in a superhistory and with importances that are independent of the fission generations, a high splitting into the thermal group, followed by fission, must in its turn be followed by a high Russian roulette, with the introduction of variance for successive fission generations. This suggests that changing the importances in future generations may be advantageous. Of course this can only be done if there is >1 fission generation in a superhistory.

6.1.2. Varying the VR according to the fission generation (10 fission generations per superhistory and tallying in all the fission generations)

A superhistory of 10 fission generations was chosen, tallying of all the responses was made in all the generations (case F) and the

Table 3

Comparison of $1/q_c$ values for functions generated with analog importances for cases D–H of PWR 2-D problem.

Case	Analog		
	$1/q_c$ fcn	$1/q_c$ est	fom_c
D	0.441	0.404	28.8
E	0.544	0.527	41.8
F	0.361	0.374	4.02
G	0.160	0.189	0.280
H	0.367	0.362	3.35

Table 4

Comparison of fom_c for optimum importances for cases E–G of PWR 2-D Problem when run with the same number of fission generations.

Case	Opt. importances
E	fom_c from a total of 50 fission generations/fom _c from 1 superhistory (Table 2)
F	0.294
G	0.577
G	0.448

cell importances were allowed to vary according to the fission generation. Two choices were made: three groups of fission generations (generations 1–3, 4–6, 7–10) with differing importances and five groups (generations 1–2, 3–4, 5–6, 7–8, 9–10). As in previous runs, analog importances were employed as the starting point. The results for the direct estimates of $1/q_c$ are shown in Table 5 including also the previous case F with one fission generation group. In Table 5, “F(10)” is the previous case with no dependence of the importances on the fission generation, “F(3–3–4)” is the case with a dependence of the importances on 3 groups of fission generations and “F(2–2–2–2–2)” is the case with a dependence of the importances on 5 groups. In contrast to previous runs, the optimization of the latter two cases was continued for another iteration (#2).

In Table 5 we note an improvement by approximately a factor of 2 after introducing a dependence of the importances on the fission generation. This demonstrates that there are transport effects within the superhistory. We see a total gain of approximately a factor of 15 (5.74/0.374) for case F(2–2–2–2–2) over the analog case.

Table 5

Comparison of direct estimates of $1/q_c$ for case F of PWR 2-D problem without and with a dependence of the importances on the fission generation.

Case	Analog (#0)	Opt. importances (#1)	Opt. importances (#2)
	$1/q_c$ est	$1/q_c$ est	$1/q_c$ est
F(10)	0.374	2.83	—
F(3-3-4)	0.354	4.90	5.26
F(2-2-2-2-2)	0.342	5.71	5.74

This gain is substantial and demonstrates the advantage of variance reduction in this problem. We note also that a fundamental tenet, beloved of deep penetration shielding practitioners, that “all neutrons are equal” looks to have been broken: in cases F(3-3-4) and F(2-2-2-2-2) identical neutrons in different fission generations are treated differently. Of course as the fission generation increases, the value of the expected future response contribution decreases.

In Tables 6–8 are shown the space/energy importances in the nine cells in the fissile region (see Fig. 6) for the cases F(1), F(3-3-4) and F(2-2-2-2-2) respectively. The energy limits of the six groups have been given in Section 6.1.1. Group 1 is the highest energy group (>500 keV).

We see that the previously-mentioned undesirable feature in case F(1) of high splitting in spatial cell 1, energy group 6 (importance 114) immediately followed by strong Russian roulette for the next fission generation group in energy group 1 (importance 1) (RR survival probability 0.0088), is softened to a survival probability of 0.08–0.09 for case F(3-3-4) and 0.06–0.11 for case F(2-2-2-2-2). Also we see lower importances in spatial cells 3–9 (see Fig. 6) as the fission generation increases in cases F(3-3-4) and F(2-2-2-2-2), as expected from the lower future detector contribution, although this is not the case in spatial cells 1 and 2. Finally we note that the importance ratios between energy groups in spatial cell 1 (that contains the local response) are far from the ratios of the expected future detector contributions. This will be discussed later.

The PWR 2-D problem has allowed us to begin to navigate in the new space defined by the new options. The results look consistent and do not exclude the employment of variance reduction within the source-iteration scheme. A gain of 15 in the figure-of-merit has been obtained. In all this we have assumed that the four quadrant global tallies for the fission heating are sufficient to maintain the fundamental mode. Problems A, C, D and H ran for more than 1 superhistory and although the results looked reasonable, a possible distortion of the fundamental mode estimate after normalization of the fission sites was not tested.

6.2. PWR 3-D

This problem is based on the previous PWR 2-D one with the same assembly configuration in the fissile region but with some axial structure (grills, etc.) and without the 1.5% variation in radial water density that provided the tilt. A height of the fissile region was specified and generic plenum zones and top and bottom plates were added, together with a bottom plate support ring. The geometry is shown in Fig. 10 where a $\frac{1}{2}$ core vertical section is shown (i.e. the right margin is the z axis). (Also the location of an ex-core neutron detector is shown in the pressure vessel well which will be the sample problem of Section 6.4.) The local response was the fission heating in an axial segment of the central pin of the central assembly.

6.2.1. Generating importances that were independent of the fission generation

Shown in Fig. 11 is the core subdivision for VR: a total of 9 zones: the central assembly containing the local response (+) then

Table 6

Space-energy cell importances in fissile region for case F(1) of PWR 2-D problem.

Spatial cell (fiss.gen.grp.)	Energy group					
	1	2	3	4	5	6
1 (1)	1	1	1	1	38	114
2 (1)	1	1	2	2	6	6
3 (1)	1	1	1	1	1	1
4 (1)	1	1	1	1	1	1
5 (1)	1	1	1	1	1	1
6 (1)	1	1	1	1	1	1
7 (1)	1	1	1	1	1	1
8 (1)	1	1	1	1	1	1
9 (1)	1	1	1	1	1	1

Table 7

Space-energy cell importances in fissile region for case F(3-3-4) of PWR 2-D problem.

Spatial cell (fiss.gen.grp.)	Energy group					
	1	2	3	4	5	6
1 (1)	1	1	4	12	12	69.1
2 (1)	1	1	2	2	2	6
3 (1)	1	1	1	1	1.67	1.67
4 (1)	1.17	1.14	1.14	1.14	1.14	1.14
5 (1)	1.32	1.14	1.14	1.14	1.14	1.14
6 (1)	1.30	1.14	1.14	1.14	1.14	1.14
7 (1)	1.18	1.14	1.14	1.14	1.14	1.14
8 (1)	1.15	1.14	1.14	1.14	1.14	1.14
9 (1)	1.14	1.14	1.14	1.14	1.14	1.14
1 (2)	5.63	5.63	5.63	5.63	22	66
2 (2)	2.81	2.81	2.81	2.81	2.81	2.81
3 (2)	0.563	0.563	0.563	0.563	0.563	1.13
4 (2)	0.563	0.563	0.563	0.563	0.563	0.563
5 (2)	0.563	0.563	0.563	0.563	0.563	0.563
6 (2)	0.563	0.563	0.563	0.563	0.563	0.563
7 (2)	0.563	0.563	0.563	0.563	0.563	0.563
8 (2)	0.563	0.563	0.563	0.563	0.563	0.563
9 (2)	0.563	0.563	0.563	0.563	0.563	0.563
1 (3)	5.17	5.17	5.17	10.3	10.3	68.8
2 (3)	1.29	1.29	1.29	1.29	1.29	1.29
3 (3)	0.205	0.205	0.205	0.205	0.205	0.409
4 (3)	0.205	0.205	0.205	0.205	0.205	0.409
5 (3)	0.205	0.205	0.205	0.205	0.205	0.409
6 (3)	0.238	0.238	0.238	0.238	0.238	0.238
7 (3)	0.238	0.238	0.238	0.238	0.238	0.238
8 (3)	0.238	0.238	0.238	0.238	0.238	0.238
9 (3)	0.238	0.238	0.238	0.238	0.238	0.238

eight rings of assemblies, each ring (approximately) a single assembly width.

As well as there being 9 radial subdivisions for VR, there were 9 axial subdivisions over the ~4 m length of the fissile region. Each of these segments had lengths between 30 and 50 cm. The central axial segment (~−20 cm < z < +30 cm) was slightly displaced from the core mid-plane because of the grills. In a first step, the central axial segment was also chosen as the axial extent of the local tally.

Thus there were 81 spatial cells in the fissile region plus 4 others outside making a total of 85. There were 6 energy groups, identical to those of problem PWR 2-D. Taking into account the 3-dimensional nature of the problem, the sub-division for “global” tallying of the fundamental mode was made as follows. Radially, the rings of Fig. 11 were combined to make 4 radial segments as shown in Fig. 12. Axially, the same central axial segment as that employed for the local tally was used, then a union of the axial sub-divisions ~−70 cm < z < −20 cm and ~+30 cm < z < +75 cm, a union of ~−120 cm < z < −70 cm and ~+75 cm < z < +125 cm and finally a union of z < −120 cm and z > +125 cm, making a total of 4 axial sub-divisions and thus a total of 16 global tallies for the fission heating, compared with the 4 in problem PWR 2-D.

Table 8

Space-energy cell importances in fissile region for case F(2-2-2-2-2) of PWR 2-D problem.

Spatial cell (fiss.gen.grp.)	Energy group					
	1	2	3	4	5	6
1 (1)	1	2	6	6	6	60
2 (1)	1	1	2	2	2	4
3 (1)	1.12	1.12	1.12	1.12	1.12	1.12
4 (1)	1.27	1.12	1.12	1.12	1.12	1.12
5 (1)	1.46	1.12	1.12	1.12	1.12	1.12
6 (1)	1.44	1.15	1.15	1.15	1.15	1.15
7 (1)	1.34	1.15	1.15	1.15	1.15	1.15
8 (1)	1.32	1.15	1.15	1.15	1.15	1.15
9 (1)	1.32	1.15	1.15	1.15	1.15	1.15
1 (2)	3.48	3.48	3.48	6.96	6.96	58.8
2 (2)	3.48	3.48	3.48	3.48	3.48	3.48
3 (2)	0.870	0.870	0.870	0.870	0.870	0.870
4 (2)	0.653	0.653	0.653	0.653	0.653	0.653
5 (2)	0.653	0.653	0.653	0.653	0.653	0.653
6 (2)	0.653	0.653	0.653	0.653	0.653	0.653
7 (2)	0.653	0.653	0.653	0.653	0.653	0.653
8 (2)	0.653	0.653	0.653	0.653	0.653	0.653
9 (2)	0.653	0.653	0.653	0.653	0.653	1.31
1 (3)	4.87	4.87	4.87	4.87	14.6	58.4
2 (3)	2.43	2.43	2.43	2.43	2.43	2.43
3 (3)	0.608	0.608	0.608	0.608	0.608	0.608
4 (3)	0.496	0.496	0.496	0.496	0.496	0.496
5 (3)	0.496	0.496	0.496	0.496	0.496	0.496
6 (3)	0.496	0.496	0.496	0.496	0.496	0.496
7 (3)	0.496	0.496	0.496	0.496	0.496	0.496
8 (3)	0.496	0.496	0.496	0.496	0.496	0.496
9 (3)	0.496	0.496	0.496	0.496	0.496	0.496
1 (4)	6.51	6.51	6.51	6.51	6.51	58.8
2 (4)	1.63	1.63	1.63	1.63	1.63	1.63
3 (4)	0.311	0.311	0.311	0.311	0.311	0.311
4 (4)	0.311	0.311	0.311	0.311	0.311	0.311
5 (4)	0.311	0.311	0.311	0.311	0.311	0.311
6 (4)	0.311	0.311	0.311	0.311	0.311	0.311
7 (4)	0.311	0.311	0.311	0.311	0.311	0.311
8 (4)	0.311	0.311	0.311	0.311	0.311	0.311
9 (4)	0.311	0.311	0.311	0.311	0.311	0.311
1 (5)	3.80	3.80	3.80	3.80	15.2	60.4
2 (5)	0.950	0.760	0.633	0.543	0.543	0.543
3 (5)	0.106	0.106	0.106	0.106	0.106	0.211
4 (5)	0.106	0.106	0.106	0.106	0.106	0.211
5 (5)	0.106	0.106	0.106	0.106	0.211	0.211
6 (5)	0.106	0.106	0.106	0.106	0.211	0.211
7 (5)	0.106	0.106	0.106	0.106	0.211	0.211
8 (5)	0.137	0.137	0.137	0.137	0.137	0.137
9 (5)	0.137	0.137	0.137	0.137	0.137	0.137

Following the PWR 2-D problem, the case F scheme was adopted (a single superhistory containing 10 fission generations) with 250,000 starting fission neutrons. In a first step, a run was made with analog importances. The importances were optimized with no dependence on the fission generation and a new run was made employing these optimized importances. The gain in the direct estimate of $1/q_c$ with the optimized importances over the analog ones was 5.3. (The predicted gain using the DSA functions generated with the analog importances was 7.8.)

In a second step, the axial extent of the local tally was reduced from $\sim -20 \text{ cm} < z < \sim +30 \text{ cm}$ to $-4 \text{ cm} < z < +4 \text{ cm}$. The importances produced from the first step were employed to generate “optimum” importances for the new case (still with no dependence on the fission generation). The functional prediction of the gain with the new importances at this step was a factor of 1.3. However the functional prediction of the gain over analog in this case was a factor of 64.8. (Note unlike the first step, a direct estimate of $1/q_c$ in a single analog run was not made – this is a prediction using the DSA functions generated with non-analog importances.) To test this prediction, 20 independent calculations were run for the

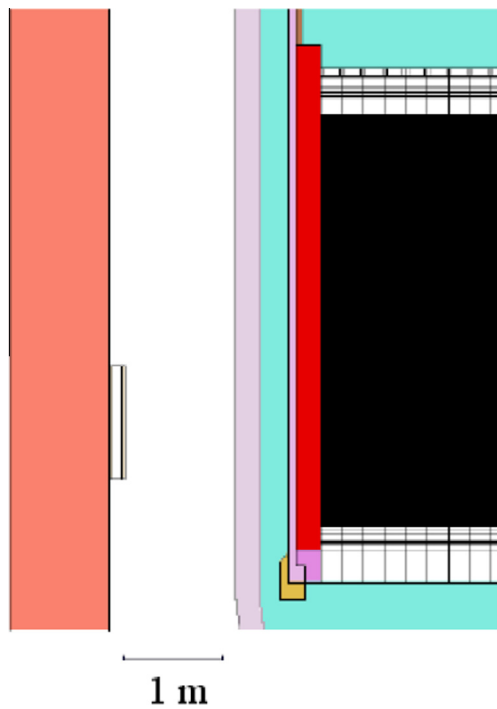


Fig. 10. PWR 3-D problem showing a 1/2 core vertical section with plena zones, top and bottom plates and ex-core detector in the PV well.

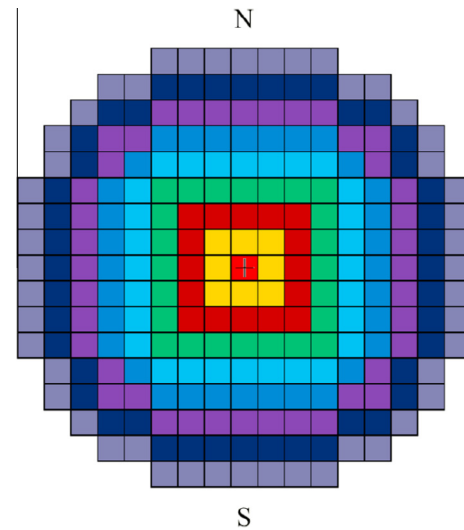


Fig. 11. PWR 3-D problem showing position of assembly with local detector and first radial core subdivision for VR.

analog case and for the optimum importances. As before, the 20 sets of results provide us with a compound figure-of-merit (fom_c) to be compared with the $1/q_c$ function values. The comparison is shown in Table 9 where we see a very satisfactory agreement.

6.2.2. Generating importances that were dependent on the fission generation

It was then desired to examine the behavior of this problem with importances that varied with the fission generation. To allow this, the number of phase space cells needed to be reduced (to overcome memory problems). This was achieved by reducing the 9 radial sub-divisions in Fig. 11 to 4 as shown in Fig. 13 and reducing the 9 axial sub-divisions to the same 4 sub-divisions as those

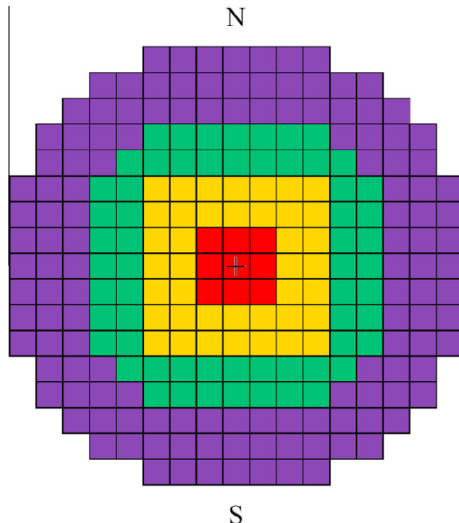


Fig. 12. PWR 3-D problem showing position of assembly with local detector and first radial core subdivision for "global" tallying.

Table 9

Comparison of function values of $1/q_c$ and fom_c for analog and optimum importances for PWR 3-D problem with 8 cm axial extent of local detector.

	Analog	Optimum importances	Opt. importances/analog
$1/q_c$ fcn	0.00899	0.582	64.8
fom_c	0.00534	0.425	79.6

used for tallying the fundamental mode, defined above. Note these axial sub-divisions create cells containing volumes that are not connected. This is not a problem. The radial sub-division for tallying the fundamental mode was also modified slightly to be, like the axial sub-division, identical to that employed to define the importances, *viz.* Fig. 13.

The calculation was made in two stages. In a first stage importances were kept independent of the fission generation. In a second stage, a dependence of the importances on the fission generation was introduced.

In the first stage, the optimum importances were arrived at in two steps as in Section 6.2.1: firstly generating optimized importances for a local tally (still the central pin of the central assembly) with a larger axial extent (~ 20 cm $< z < \sim +30$ cm) employing analog importances; secondly using these importances when the axial extent is reduced to 8 cm (slightly different from previously: $+1$ cm $< z < +9$ cm instead of -4 cm $< z < +4$ cm). The first step yielded a predicted gain of 6.1 in the $1/q_c$ value (compare 7.8 previously). Employing the resultant importances in the second step with the axially reduced local detector and performing the optimization, yielded a predicted (i.e. with the DSA functions) gain of a factor of 1.22 (compare 1.28 previously) and a predicted gain over analog of 54.6 (compare 64.8 previously). (Because of the grosser spatial cell binning compared with previously, it is not surprising that there is a small impact on $1/q_c$).

In the second stage the optimum importances, resulting from the above, the same for all fission generations, were employed in a run that allowed a dependence of the importances on the fission generation with 5 groups of generations, *viz.* 1-2, 3-4, 5-6, 7-8, 9-10. Optimized importances were generated in these 5 fission generation groups and were employed in a final run. With the new importances, there was a gain in the direct estimate of $1/q_c$ of a factor of 1.99. This is close to the gain obtained in the PWR 2-D problem (Table 5).

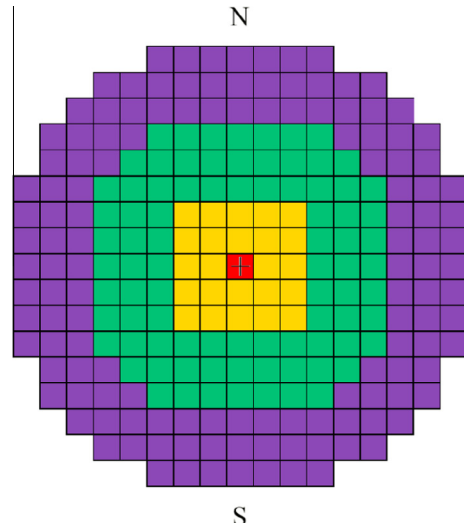


Fig. 13. PWR 3-D problem showing position of assembly with local detector and second radial core subdivision for both VR and "global" tallying.

The final importances in each of the 5 fission generation groups are shown in Table 10. We see again the two effects noted in the PWR 2-D problem: in the cell that contains the local detector, a softening of the Russian roulette of the fission neutrons between fission generation groups and lower importances in spatial cells that are not too close to the local detector as the fission generation increases.

6.2.3. Generating importances that were dependent on the fission generation with the classic importance formalism

The procedure followed in Section 6.2.2 was repeated using the weighted expected future detector contributions (ϕ_*) to define the cell importances in a closely analogous fashion to Solomon et al. (2009). After the first stage (with cell importances that were independent of the fission generation) the $1/q_c$ value was a factor of 11.7 poorer than at the same point in Section 6.2.2. Then allowing the cell importances to vary according to the same 5 fission generation groups improved $1/q_c$ by a factor of 2.2. The quality remained thus a factor of slightly over an order of magnitude lower compared with the results of Section 6.2.2.

The final importances in each of the 5 fission generation groups are shown in Table 11. For purposes of comparison with the values in Table 10, they have been normalized so that the importance in generation group 1, energy group 1, radial cell 1 and axial cell 1 is the same (we can do this as splitting/RR employs ratios of the importances). We remind ourselves that, as discussed in Solomon et al. (2009), the values in Table 11 are proportional to an importance function for a tally that is composed of a number of tallies, each normalized by its estimated mean.

The following important differences between the results in Tables 10 and 11 may be noted:

- For the classic importances, the variation within each fission generation group looks reasonably similar for all generation groups. Instead for the DSA importances, the variation within the first fission generation group looks quite different from that within the other four groups.
- In the fission generation groups 2-5 there looks to be a somewhat greater decrease in the classic importances in the higher energy groups as one moves away, radially and axially, from the local detector compared with the DSA importances.

Table 10

Space-energy cell importances in fissile region for case (2-2-2-2-2) of PWR 3-D problem.

Fiss. gen. gp.	Radial cell (Fig. 13)	Axial cell	Energy group					
			1	2	3	4	5	6
1	1	1	0.946	1.89	7.57	7.57	174	341
1	1	2	1	1	6	8	8	8
1	1	3	0.974	0.974	8	8	16	16
1	1	4	0.846	1.69	5.08	15.2	15.2	15.2
1	2	1	0.946	1.89	3.79	7.57	7.57	7.57
1	2	2	1	1	1	2	2	4
1	2	3	0.974	0.974	2	2	2	4
1	2	4	0.846	1.69	1.69	1.69	1.69	5.08
1	3	1	1.48	1.48	1.39	1.39	1.39	1.39
1	3	2	1.94	1.53	0.689	0.689	0.689	1.38
1	3	3	1.86	1.40	1.02	1.02	1.02	1.02
1	3	4	1.56	1.35	0.846	0.846	0.846	1.69
1	4	1	2.08	1.50	1.03	1.03	1.03	1.03
1	4	2	2.31	1.53	0.689	0.689	0.689	0.689
1	4	3	2.20	1.49	0.716	0.716	0.716	0.716
1	4	4	1.90	1.33	0.846	0.846	0.846	0.846
2	1	1	24.2	24.2	24.2	24.2	72.7	477
2	1	2	2.02	4.04	4.04	4.04	14.4	14.4
2	1	3	2.17	2.17	2.17	13.0	13.0	13.0
2	1	4	2.23	2.23	2.23	2.23	11.1	22.3
2	2	1	4.04	4.04	4.04	4.04	4.04	8.08
2	2	2	2.02	2.02	2.02	2.02	3.60	3.60
2	2	3	2.17	2.17	2.17	2.17	2.17	4.33
2	2	4	2.23	2.23	2.23	2.23	4.46	4.46
2	3	1	0.808	0.705	0.705	0.705	0.705	1.41
2	3	2	0.461	0.461	0.461	0.461	0.461	0.921
2	3	3	0.542	0.542	0.542	0.542	0.542	1.08
2	3	4	0.557	0.557	0.557	0.557	0.557	1.11
2	4	1	0.487	0.487	0.487	0.487	0.487	0.975
2	4	2	0.323	0.323	0.323	0.323	0.323	0.645
2	4	3	0.323	0.323	0.323	0.323	0.645	0.645
2	4	4	0.339	0.339	0.339	0.339	0.679	0.679
3	1	1	4.04	4.04	16.2	16.2	32.3	343
3	1	2	3.29	3.29	3.29	13.2	13.2	13.2
3	1	3	1.64	1.64	6.58	6.58	13.2	13.2
3	1	4	2.05	2.05	13.2	13.2	13.2	13.2
3	2	1	4.04	4.04	4.04	4.04	4.04	4.04
3	2	2	1.64	1.64	1.64	1.64	1.64	3.29
3	2	3	1.64	1.64	1.64	1.64	3.29	3.29
3	2	4	2.05	2.05	2.19	2.19	4.38	4.38
3	3	1	0.505	0.505	0.505	0.505	0.505	1.01
3	3	2	0.386	0.353	0.353	0.353	0.353	0.706
3	3	3	0.411	0.411	0.411	0.411	0.411	0.822
3	3	4	0.411	0.411	0.411	0.411	0.822	0.822
3	4	1	0.475	0.475	0.475	0.475	0.475	0.475
3	4	2	0.238	0.235	0.235	0.235	0.471	0.471
3	4	3	0.238	0.235	0.235	0.235	0.471	0.471
3	4	4	0.271	0.271	0.271	0.271	0.542	0.542
4	1	1	4.01	4.01	24.1	24.1	24.1	356
4	1	2	2.50	2.50	2.50	9.99	9.99	9.99
4	1	3	1.49	1.49	1.49	11.9	11.9	11.9
4	1	4	5.95	5.95	5.95	5.95	5.95	20.8
4	2	1	4.01	4.01	4.01	4.01	4.81	4.81
4	2	2	1.25	1.25	1.25	1.25	1.25	2.50
4	2	3	1.49	1.49	1.49	1.49	1.49	2.50
4	2	4	1.49	1.49	1.49	2.98	2.98	2.98
4	3	1	0.375	0.375	0.375	0.375	0.375	0.749
4	3	2	0.250	0.208	0.208	0.208	0.416	0.416
4	3	3	0.250	0.248	0.248	0.248	0.496	0.496
4	3	4	0.264	0.264	0.264	0.264	0.527	0.527
4	4	1	0.313	0.313	0.313	0.313	0.313	0.313
4	4	2	0.156	0.156	0.156	0.156	0.313	0.313
4	4	3	0.156	0.156	0.156	0.156	0.313	0.313
4	4	4	0.166	0.166	0.166	0.166	0.332	0.332
5	1	1	3.61	14.5	14.5	14.5	57.8	458
5	1	2	2.36	2.36	3.15	3.15	9.45	9.45
5	1	3	2.45	2.86	2.86	5.72	11.4	11.4
5	1	4	2.45	2.45	11.3	11.3	11.3	11.3
5	2	1	1.81	1.81	1.81	1.81	1.81	3.08
5	2	2	0.787	0.787	0.787	0.787	0.787	1.35
5	2	3	0.817	0.817	0.817	0.817	0.817	1.63

Table 10 (continued)

Fiss. gen. gp.	Radial cell (Fig. 13)	Axial cell	Energy group					
			1	2	3	4	5	6
5	2	4	0.817	0.817	0.817	0.817	1.61	1.61
5	3	1	0.191	0.191	0.191	0.191	0.191	0.382
5	3	2	0.112	0.112	0.112	0.112	0.112	0.225
5	3	3	0.117	0.117	0.117	0.117	0.233	0.233
5	3	4	0.137	0.137	0.137	0.137	0.137	0.274
5	4	1	0.152	0.152	0.152	0.152	0.152	0.152
5	4	2	0.0740	0.0740	0.0740	0.0740	0.148	0.148
5	4	3	0.0740	0.0740	0.0740	0.0740	0.148	0.148
5	4	4	0.0764	0.0764	0.0764	0.0764	0.153	0.153

- For the DSA importances the low energy value is greater than the high energy value by a substantial factor, especially near the local detector, compared with the classic importances. (Compare the values for radial cell 1, axial cell 1 for any fission generation group in Table 10 with the analogous values in Table 11.)

The last point looks to be the most important difference, with, the classic importances reflecting a combination of future expected detector contributions for a nearly critical system, where, corresponding to our intuition, we expect there not to be a great variation with energy.

At present we are unable to explain the differences in results between the DSA approach and the classic formalism. However two points may be made:

- (1) As discussed in Booth and Burn (1993) and Burn (1996) and at greater length in Booth (2012), when there is a small probability of a detector contribution from the last splitting surface, the classic approach may give results that are far from optimum. However in the examples given in these references, the classic approach splits more than the DSA, whilst here the opposite is the case.
- (2) Within a superhistory, there are numerous correlations between tracks that come from the same split progeny at space/energy surfaces, between tracks that come from the same progeny at natural bifurcation events (i.e. fissions) and between detector contributions from different fission generations. All these correlations are taken into account with the DSA (Burn, 1995). In particular it was noted that, unlike fixed source shielding problems, the correlations resulting from the same neutron giving detector contributions in different fission generations was an important component of the second moment (>50%). Such effects are not included in the classic approach. One expects that these effects will have an impact on the phase space cell importances. However they usually reduce the splitting whilst the opposite is the case here.

6.2.4. Verifying that the fundamental mode is maintained

We return to the approach of Section 6.2.1 with importances that are independent of the fission generation – and adopt the importances that provided a predicted gain of $1/q_c$ over analog of 64.8 and a real gain of fom_c over analog of 79.6 (Table 9). These importances were defined on 81 spatial cells in the fissile region and 6 energy groups. They have not been shown here but we may mention that the maximum value in group 6 at the local tally was 1010 with the value in group 1 at the same location: 2. The minimum value, in the outer assembly ring, was 0.35.

Three runs were made, all starting from the same fundamental mode estimate as that used previously and employing 250,000 starting neutrons per superhistory. One run used a superhistory

of 10 fission generations, 250 superhistories and the above, “optimum” DSA, importances. The second run was identical but employed analog importances. The third run was standard, analog, MCNP, therefore (implicitly) one fission generation per superhistory, and 2500 generations.

The Shannon entropy is a measure of the dispersion of the fission sites (X-5 Monte Carlo Team, 2005, Vol. I, Ch. 2, pp. 2–179 to 2–180). It was defined over a mesh consisting radially of 17×17 bins (i.e. 1 bin per assembly, with 48 of the 289 radial bins outside the fission region – see Fig. 11) and axially of 40 bins (each mesh having a height of just over 10 cm), making a total of 9640 meshes in the fissile region. The variation of the Shannon entropy in each calculation, from start to finish, is shown in Fig. 14. The Shannon entropy in the standard MCNP run is shown only for every 10 fission generations, so that there is an approximately equal effort between each point in Fig. 14 in all three cases.

There looks in Fig. 14 to be good agreement between the standard MCNP results and the DSA analog importance run, as expected. We see that the runs with 10 fission generations per superhistory both look to vary reasonably around their respective means. The run with the optimized importances, exhibits a variation that, as expected, is larger than that with analog importances (after 250 superhistories, the fsd of the analog run was 0.000035 and of the optimized importance run was 0.000058). There is however a difference in the two means (12.980 and 12.924 respectively) that is clearly a signal. Although the major result here is the maintenance of the fundamental mode with the optimized importances, with a variance that is higher than the analog case, the different mean from the analog case was unexpected.

This effect was further investigated. It was found that the optimized importances in the three outer assembly rings (see Fig. 11) were responsible for the altered mean. The difference between these importances and those in the six inner assembly rings was that in the latter case the importance in energy group 1 (>500 keV) was less than that in energy group 6 (<1 eV) (in the same spatial cell), whilst in the former case the opposite was the case with the importance in energy group 1 being 2–3 times greater than that in energy group 6. Thus for the three outer rings, as there is a high probability of neutrons remaining within the same spatial cell within a fission generation, neutrons suffer Russian roulette before undergoing fission. This Russian roulette and consequent lower number of candidate fission sources in these rings was assumed to be the cause of the lowering of the Shannon entropy mean.

To verify this, we chose one of these rings – the third from the outside – and, keeping the importances in the rest of the geometry analog, ran three cases:

- test case I: importances in groups 4–6 (<5 keV), 1/100 of the importances in groups 1–3;
- test case II: importances in groups 4–6, 1/10 of the importances in groups 1–3;

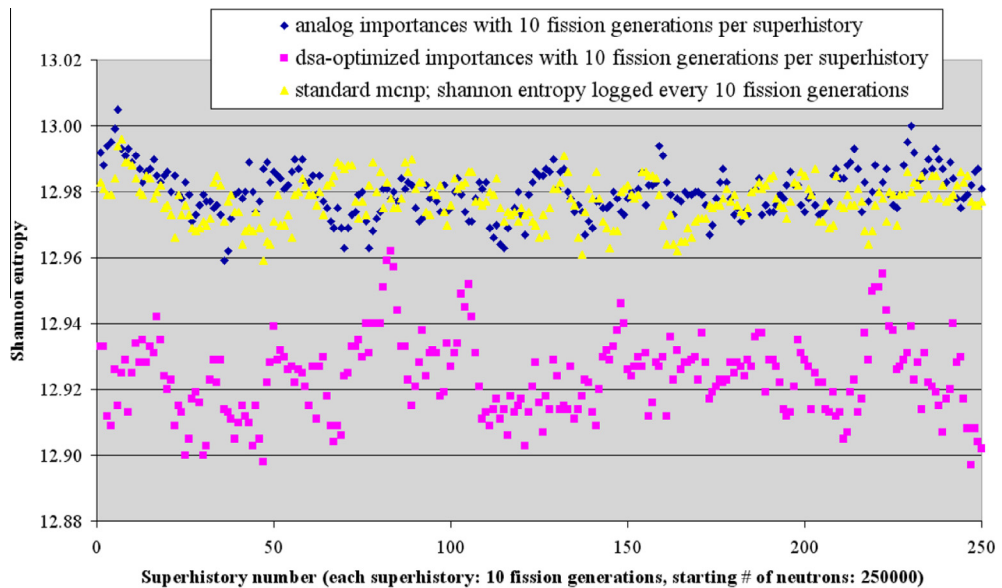
Table 11

Space-energy cell importances in fissile region for case (2-2-2-2-2) of PWR 3-D problem generated with the classic importance formalism.

Fiss. gen. gp.	Radial cell (Fig. 13)	Axial cell	Energy group					
			1	2	3	4	5	6
1	1	1	0.946	1.15	1.03	0.990	1.29	0.912
1	1	2	0.244	0.287	0.244	0.183	0.205	0.233
1	1	3	0.310	0.294	0.261	0.254	0.263	0.241
1	1	4	0.478	0.532	0.433	0.370	0.403	0.450
1	2	1	0.102	0.122	0.0557	0.0503	0.0596	0.0680
1	2	2	0.0460	0.0512	0.0257	0.0239	0.0243	0.0269
1	2	3	0.0482	0.0532	0.0276	0.0258	0.0272	0.0310
1	2	4	0.0749	0.0941	0.0433	0.0407	0.0408	0.0452
1	3	1	0.0128	0.00631	0.00769	0.00636	0.00660	0.00734
1	3	2	0.00877	0.00462	0.00433	0.00675	0.00467	0.00522
1	3	3	0.00857	0.00481	0.00498	0.00576	0.00490	0.00552
1	3	4	0.0122	0.00601	0.00754	0.00601	0.00670	0.00759
1	4	1	0.00754	0.00405	0.00381	0.00690	0.00441	0.00461
1	4	2	0.00522	0.00255	0.00242	0.00450	0.00256	0.00291
1	4	3	0.00507	0.00257	0.00253	0.00454	0.00280	0.00312
1	4	4	0.00700	0.00297	0.00294	0.00455	0.00310	0.00341
2	1	1	0.493	0.729	0.576	0.434	0.710	0.567
2	1	2	0.230	0.293	0.175	0.177	0.185	0.204
2	1	3	0.146	0.200	0.169	0.214	0.217	0.204
2	1	4	0.320	0.380	0.349	0.329	0.356	0.258
2	2	1	0.0462	0.116	0.0503	0.0485	0.0527	0.0591
2	2	2	0.0214	0.0411	0.0223	0.0199	0.0194	0.0215
2	2	3	0.0249	0.0439	0.0225	0.0230	0.0226	0.0237
2	2	4	0.0412	0.0813	0.0385	0.0397	0.0389	0.0425
2	3	1	0.00616	0.00572	0.00705	0.00581	0.00591	0.00641
2	3	2	0.00393	0.00346	0.00336	0.00522	0.00356	0.00406
2	3	3	0.00419	0.00379	0.00397	0.00458	0.00385	0.00447
2	3	4	0.00611	0.00507	0.00675	0.00542	0.00537	0.00611
2	4	1	0.00402	0.00390	0.00380	0.00695	0.00422	0.00440
2	4	2	0.00242	0.00210	0.00206	0.00392	0.00221	0.00245
2	4	3	0.00250	0.00232	0.00230	0.00401	0.00251	0.00264
2	4	4	0.00352	0.00323	0.00349	0.00475	0.00328	0.00375
3	1	1	0.352	0.700	0.432	0.724	0.517	0.493
3	1	2	0.146	0.172	0.173	0.156	0.150	0.177
3	1	3	0.133	0.192	0.164	0.157	0.169	0.141
3	1	4	0.212	0.276	0.273	0.254	0.315	0.233
3	2	1	0.0512	0.113	0.0448	0.0425	0.0423	0.0408
3	2	2	0.0184	0.0324	0.0174	0.0150	0.0157	0.0165
3	2	3	0.0198	0.0335	0.0187	0.0183	0.0183	0.0193
3	2	4	0.0322	0.0675	0.0329	0.0283	0.0289	0.0300
3	3	1	0.00527	0.00477	0.00616	0.00503	0.00483	0.00567
3	3	2	0.00290	0.00255	0.00244	0.00378	0.00252	0.00296
3	3	3	0.00303	0.00277	0.00293	0.00340	0.00287	0.00303
3	3	4	0.00491	0.00441	0.00586	0.00476	0.00483	0.00512
3	4	1	0.00356	0.00329	0.00319	0.00562	0.00346	0.00350
3	4	2	0.00204	0.00184	0.00174	0.00332	0.00194	0.00207
3	4	3	0.00199	0.00186	0.00178	0.00319	0.00202	0.00202
3	4	4	0.00303	0.00277	0.00278	0.00430	0.00282	0.00291
4	1	1	0.277	0.442	0.481	0.382	0.421	0.348
4	1	2	0.127	0.159	0.135	0.144	0.161	0.165
4	1	3	0.109	0.172	0.146	0.150	0.166	0.124
4	1	4	0.185	0.335	0.257	0.271	0.306	0.224
4	2	1	0.0289	0.0552	0.0276	0.0247	0.0266	0.0257
4	2	2	0.0144	0.0248	0.0130	0.0110	0.0122	0.0136
4	2	3	0.0138	0.0243	0.0131	0.0124	0.0127	0.0129
4	2	4	0.0239	0.0503	0.0228	0.0227	0.0237	0.0233
4	3	1	0.00378	0.00336	0.00430	0.00360	0.00365	0.00339
4	3	2	0.00202	0.00176	0.00172	0.00270	0.00175	0.00181
4	3	3	0.00212	0.00195	0.00202	0.00232	0.00199	0.00196
4	3	4	0.00350	0.00337	0.00436	0.00351	0.00329	0.00329
4	4	1	0.00284	0.00249	0.00221	0.00424	0.00256	0.00250
4	4	2	0.00142	0.00128	0.00123	0.00236	0.00135	0.00128
4	4	3	0.00144	0.00134	0.00130	0.00225	0.00144	0.00128
4	4	4	0.00229	0.00210	0.00214	0.00327	0.00221	0.00213
5	1	1	0.406	0.636	0.670	0.611	0.596	0.165
5	1	2	0.0586	0.0833	0.0843	0.0803	0.0926	0.0685
5	1	3	0.0581	0.106	0.0921	0.0971	0.117	0.0611
5	1	4	0.118	0.173	0.157	0.192	0.208	0.127
5	2	1	0.0146	0.0277	0.0130	0.0120	0.0120	0.0103
5	2	2	0.00641	0.0118	0.00572	0.00522	0.00542	0.00440
5	2	3	0.00655	0.0117	0.00660	0.00586	0.00586	0.00458

Table 11 (continued)

Fiss. gen. gp.	Radial cell (Fig. 13)	Axial cell	Energy group					
			1	2	3	4	5	6
5	2	4	0.0120	0.0249	0.0116	0.0109	0.0110	0.00892
5	3	1	0.00207	0.00223	0.00287	0.00237	0.00231	0.00134
5	3	2	0.00103	0.000852	0.000833	0.00136	0.000872	0.000621
5	3	3	0.00118	0.00116	0.00123	0.00141	0.00117	0.000764
5	3	4	0.00185	0.00193	0.00246	0.00188	0.00183	0.00105
5	4	1	0.00140	0.00150	0.00147	0.00258	0.00144	0.000798
5	4	2	0.000759	0.000680	0.000650	0.00123	0.000685	0.000407
5	4	3	0.000788	0.000734	0.000749	0.00137	0.000813	0.000477
5	4	4	0.00122	0.00130	0.00136	0.00208	0.00144	0.000695

**Fig. 14.** PWR 3-D problem of Sec. 6.2.1: variation of Shannon entropy for analog and optimized importances independent of the fission generation and comparison with standard MCNP.

- test case III: importances in groups 4–6, 10 times the importances in groups 1–3.

A superhistory of 10 fission generations was used, 250,000 starting neutrons in each superhistory and 50 superhistories. The variation of the Shannon entropy over the 50 superhistories is shown in Figs. 15a and 15b. We see in these figures that it is indeed the Russian roulette in the phase space cell where fission occurs that lowers the mean of the Shannon entropy whilst splitting in the same cell does not change it. The reason is that the Russian roulette introduces variance into the generation of fission sites at the next normalization point (i.e. end of superhistory).

A lower mean of the Shannon entropy does not necessarily imply a distortion in one direction (i.e. bias) in the fundamental mode – a deviation from the smoothness of the fundamental distribution either “up” or “down” at the end of different superhistories will in both cases lower the Shannon entropy. Thus the results are consistent with a greater noise associated with the distribution of fission sites without this necessarily involving a distortion of the fundamental mode.

As the maintenance of the fundamental mode when variance reduction is applied is a cornerstone of the paper, it was desired to make a further analysis. Instead of examining selected 2-D radial or axial power profiles to determine whether the

distribution varied or not from the fundamental mode, the following approach was adopted:

1000 superhistories, each of 10 fission generations, were run, starting from a converged fundamental mode, with 500,000 starting neutrons per superhistory (compare previously 250 superhistories and 250,000 starting neutrons per superhistory). For the first half of the calculation (500 superhistories), analog importances were employed. For the second half, various options were used which will be described in the next paragraph. In each half of the calculation, the fission sites at the end of each superhistory were scored in the same meshes as those used for the Shannon entropy (a total of 9640). For each mesh, a mean and a standard deviation (SD) (computed between superhistories) were calculated over the first and second halves of the calculation. The difference of the two means was computed together with its SD, assuming independence and normality of the two samples. The difference and its SD were compared for each of the 9640 meshes and the fraction of the 9640 differences lying within 1, between 1 and 2, between 2 and 3, between 3 and 4, ... SD's was logged. (For example if the fission sites at the end of each superhistory in each half of the calculation are normal, independent and identical distributions (IID's) (i.e. with the same mean) then the difference is normally distributed around a mean of zero and the fractions will be close to: 0.6827, 0.2718, 0.04280, 0.002637,) An example of a single mesh is given in the following sketch (two normal distributions with different means):

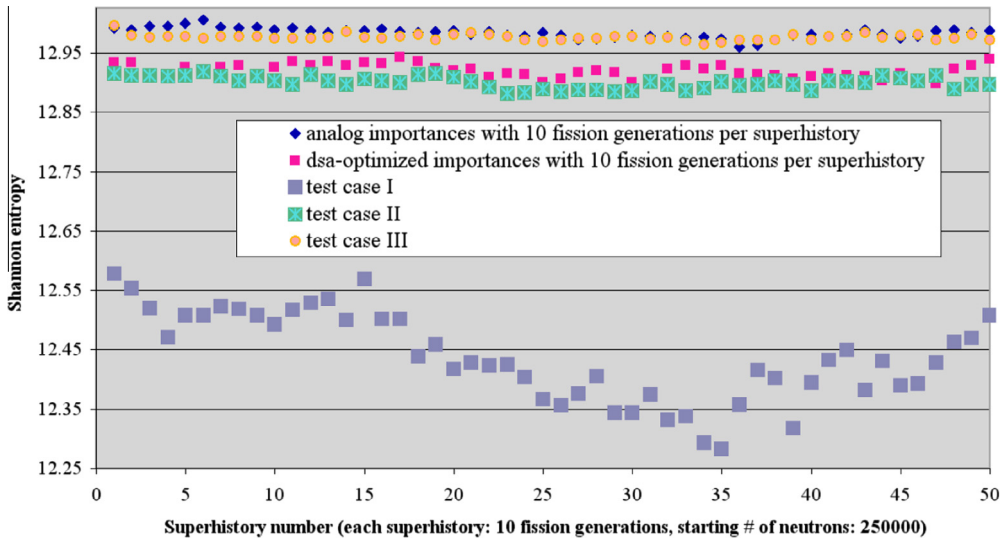


Fig. 15a. PWR 3-D problem of Sec. 6.2.1: variation of Shannon entropy over 50 superhistories (500 fission generations) for test cases and comparison with analog and optimized importances.

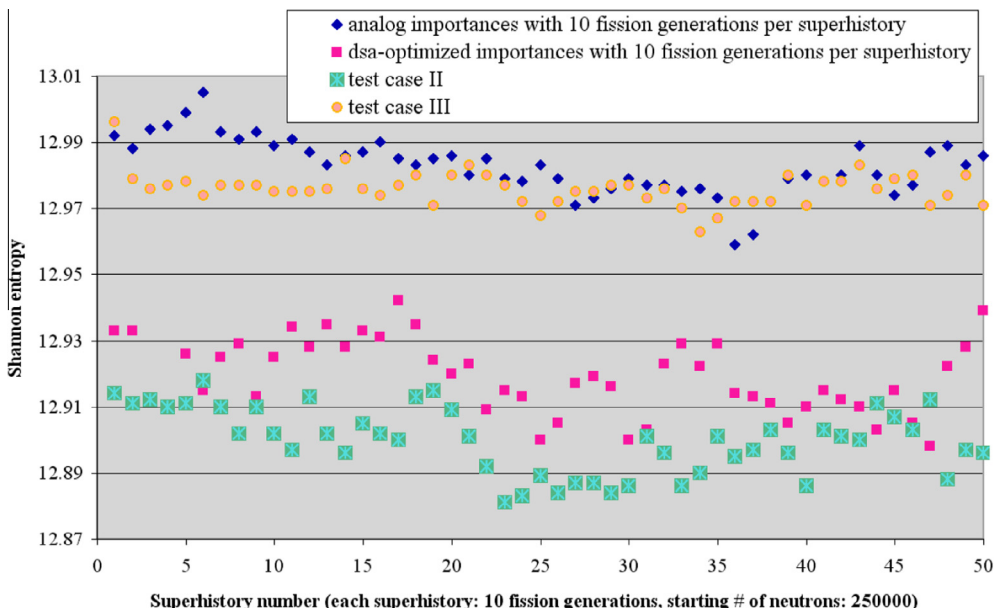
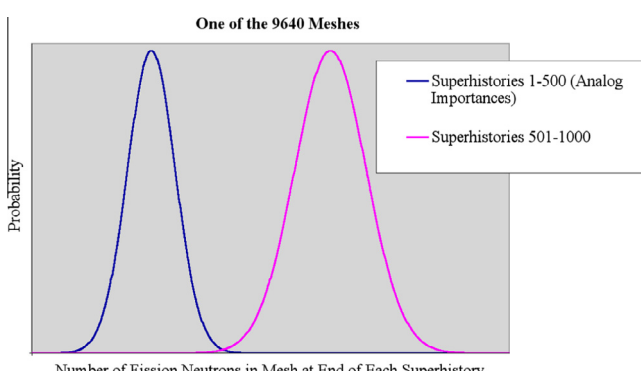


Fig. 15b. PWR 3-D problem of Sec. 6.2.1: variation of Shannon entropy over 50 superhistories (500 fission generations) for test cases and comparison with analog and optimized importances (increased scale of y axis).



The various options for the 500 superhistories of the second half of each calculation were: analog importances, optimum impor-

tances (as found with the DSA), test cases I and II (see above) and analog importances but with an artificial absorption in the central assembly (see Fig. 11) over the whole height of the fissile region, characterized by applying a kill probability of 0.25 to every neutron the first time it appeared below 1 eV. Thus the last option distorts the fundamental mode, the first option does not, and the 2nd, 3rd and 4th options, involving variance reduction, may or may not distort the fundamental mode.

The analog importance results are shown in Fig. 16 where they are compared with the differences between two normal IID's. We see that the differences between the 1st and 2nd halves of the calculation are actually quite far from normal: the first five values for normal IID's are: 0.683, 0.272, 0.0428, 0.00264 and 0.0000628 whilst the analog-analog results are: 0.535, 0.327, 0.114, 0.0226 and 0.00156. Such differences are assumed to be due to the collective behavior arising from the loosely-coupled nature of the problem, referred to in the introductory part of Section 6.

Fig. 17 compares normal IID differences and analog-analog differences with the three VR schemes and with the artificial absorption. The artificial absorption case shows clear distortions as expected. Test case I (1/100 Russian roulette survival probability) shows probable distortions as one might deduce from the instability of the Shannon entropy over 50 superhistories in **Fig. 15a**. The test case II and optimum importance results instead are quite near the analog results. One therefore infers that these cases do not distort the fundamental mode.

The same analysis was then applied to the problem of Section 6.2.2 (importances that were a function of the fission generation with 5 fission generation groups), comparing normal IID differences, analog-analog and analog-optimum importance differences. (We remind ourselves that the optimum importances are those shown in **Table 10**.) The results are shown in **Fig. 18**, where we see excellent results for the optimum importances compared with the analog differences. Note in **Figs. 16–18** all non-zero stochastic results are shown.

6.3. Liquid lead-cooled FR

This problem is based loosely on the ELSY design (Cinotti et al., 2008). A radial section of the core assembly configuration (fissile region only) is shown in **Fig. 19**. (Note the 6 gray assemblies

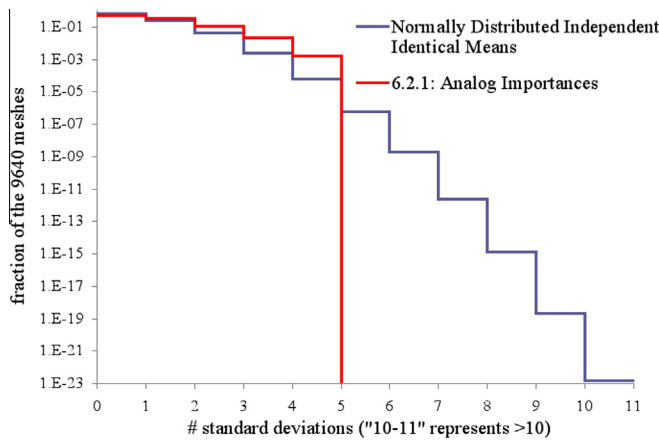


Fig. 16. PWR 3-D problem of Sec. 6.2.1: measure of the maintenance of the fundamental mode; analog-analog.

toward the periphery do not contain fissile material.) The local tally was chosen as the fission heating in an axial segment ± 1.5 cm around the core mid-plane in a single pin of the right-hand of the two central assemblies. This pin in its assembly is shown in **Fig. 20**. The global tallies are the 5 fissile zones shown in **Fig. 19** and are identical to the radial sub-division in the core to form the spatial cells.

Although the axial extent of the local tally is just 3 cm, the height of the fissile region is only just over 90 cm (see **Fig. 21**). No axial sub-division of the fissile region was made either for VR or for tallying the fundamental mode. Thus there were just 5 cells in the fissile region plus one outside and 5 tallies for the fundamental mode. The same 6 energy groups were employed for VR as in the previous sample problems, viz. with limits 500 keV, 50 keV, 5 keV, 100 eV and 1 eV.

The scheme: 1 superhistory containing 10 fission generations was employed with 250,000 starting neutrons. At first no dependence of the cell importances on the fission generation was allowed, then the 5 fission generation group scheme 2-2-2-2-2 was used, finally each of the 10 fission generations was given its own importances.

The starting importances employed had already been partially optimized in previous test runs so they were substantially better

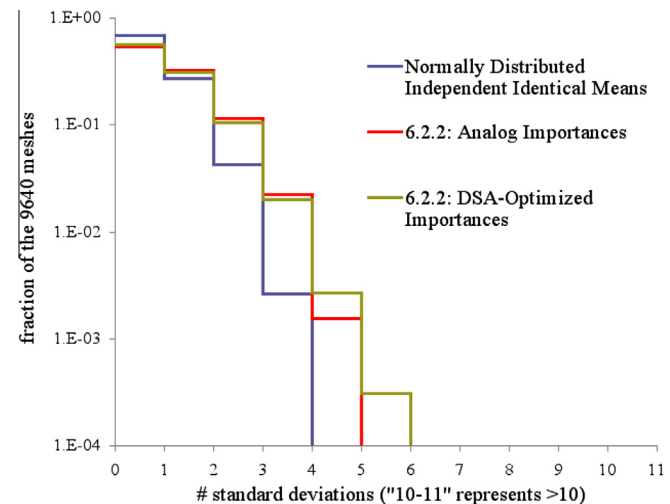


Fig. 18. PWR 3-D problem of Sec. 6.2.2: measure of the maintenance of the fundamental mode; analog-analog, analog-optimum importances.

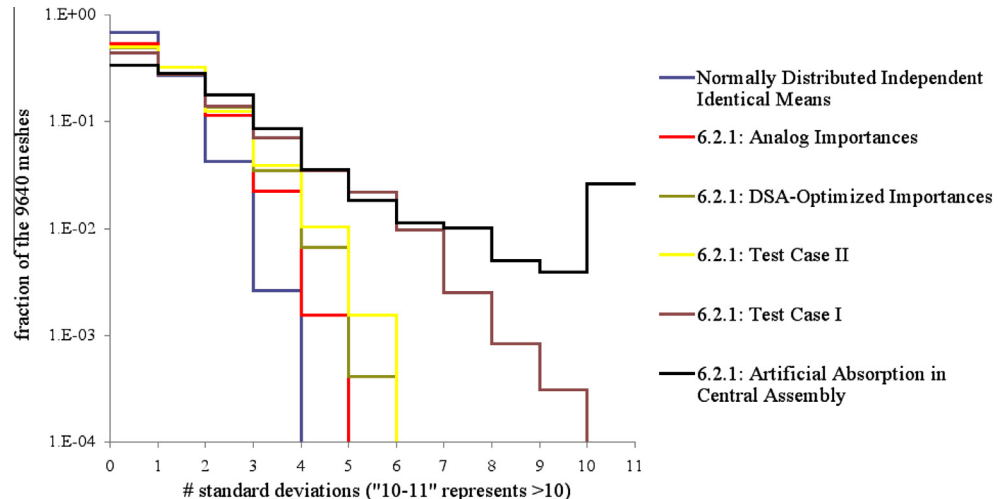


Fig. 17. PWR 3-D problem of Sec. 6.2.1: measure of the maintenance of the fundamental mode; analog-analog, analog-3 VR options, analog-artificial absorption.

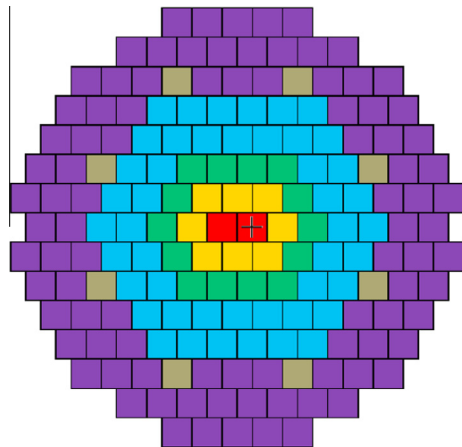


Fig. 19. Lead-cooled FR problem showing assembly configuration and radial core subdivision for VR.

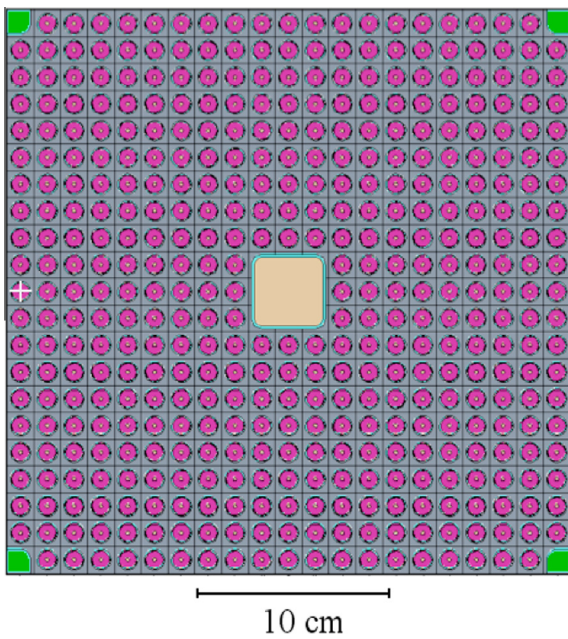


Fig. 20. Lead-cooled FR problem showing pin (marked with cross) on left side of right hand central assembly employed as the local detector.

than analog. A number of steps were executed with the importances generated at one step being employed at the next step. Table 12 shows the various $1/q_c$ values: direct estimates ($1/q_c$ est), function values for analog importances ($1/q_c$ fcn anal), function values for the importances employed at each step ($1/q_c$ fcn run) and the predicted optimum function values ($1/q_c$ fcn opt) at each step. In Table 12, “ f_{gg} run/opt” denotes the number of fission generation groups for the importance dependency, “run” used in the step and “opt” in the optimum importances generated from that step.

In Table 12 we see that the starting importances were already near-optimum (for importances independent of the fission generation). We also see that there is good agreement between the direct estimate of $1/q_c$ at one step and the predicted optimum function value at the preceding step. Finally we note that the dependence 2-2-2-2 provides an approximate factor 2 improvement over importances that are independent of the fission generation, similar to the PWR problems. Allowing a different importance dependence for each fission generation, i.e. 1-1-1-1-1-1-1-1 yields a further improvement of ~15%.

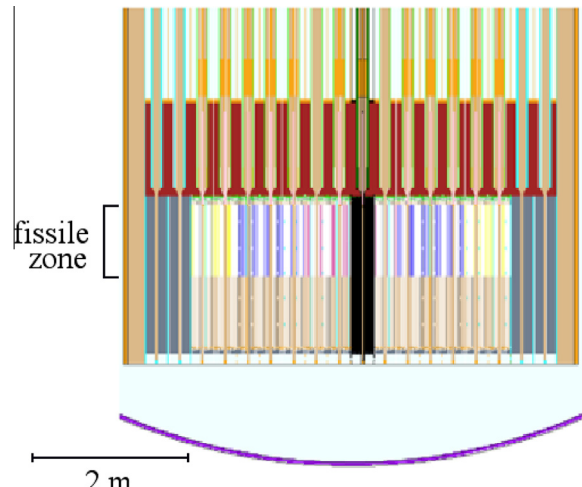


Fig. 21. Lead-cooled FR problem showing a full core vertical section with fissile region, plena zones, nozzle zones, etc. above and below fissile region.

The space-energy cell importances for the case 2-2-2-2-2 (output from step 3 in Table 12) are shown in Table 13. In Table 13 the spatial cell 6 is everything outside the fissile region and the values “-1” signify that an insufficient number of scores were made to construct a reasonable estimate of compound squares of the future expected detector contributions for that cell. Comparing the values in Table 13 with those in Tables 10 and 8 we note that:

- as expected for a fast problem, the maximum importances are shifted up in energy to above 100 eV with very low values below 1 eV.
- there are higher importances in fission generation groups after the first one, compared with the PWR 2-D and 3-D problems. This results in a further softening of the Russian roulette between neutrons entering fission in one generation group and neutrons born from fission in the next generation group. One might infer that this is due to the greater transport of neutrons between fissions in the FR problem, i.e. it is more strongly coupled compared with the previous two thermal problems. Notwithstanding, the gain in quality in going from 1 to 5 generation groups is similar in all three problems.

6.4. PWR 3-D ex-core

Now we define the local detector as being outside the core. It is convenient to employ the previous PWR 3-D problem using as local response, the $^{10}\text{B}(n,\alpha)$ rate in an ex-core neutron detector placed in the PV well (Burn et al., 2012) (see Fig. 10). A radial section at the height of the detector is shown in Fig. 22.

Shown in Fig. 23 is the core subdivision for VR: a total of 9 zones with the ex-core detector being in the East direction. In the previous sample problems the color coding and shading (light red: hottest; dark blue: coldest) was directed at the local tally and the importance direction was evident. Instead here the order is not *a priori* obvious (apart from the hottest zone). [Neither is it obvious *a posteriori* from the optimum cell importances because of the compound response (local + global components).]

As can be seen from Fig. 10 the ex-core detector is opposite the lower axial part of the fissile region. Therefore a vertical division was made approximately 30 cm above the core mid-plane and the above 9 zones were divided into 18 cells – 9 above and 9 below. Then a further 31 cells were employed to sub-divide the geometry

Table 12Comparison of direct estimates and function values of $1/q_c$ for lead-cooled FR problem.

Step	fgg run	fgg opt	$1/q_c \text{ est.}$	$1/q_c \text{ fcn anal}$	$1/q_c \text{ fcn run}$	$1/q_c \text{ fcn opt.}$	$q_c \text{ fcn run}/q_c \text{ fcn opt}$	$q_c \text{ fcn anal}/q_c \text{ fcn opt}$
1	1	1	0.20	0.022	0.19	0.22	1.1	9.9
2	1	5	0.17	0.019	0.15	0.32	2.1	17
3	5	5	0.38	0.023	0.33	0.38	1.2	17
4	5	10	0.34	0.022	0.31	0.41	1.3	19
5	10	10	0.40	0.021	0.35	0.40	1.2	19
6	10	10	0.46	0.026	0.38	0.42	1.1	17

Table 13

Space-energy cell importances in fissile region for case (2-2-2-2-2) of lead-cooled FR problem.

Spatial cell (fis. gen. gp.)	Energy group					
	1	2	3	4	5	6
1 (1)	1.77	5.58	12.7	38.0	0.445	-1
2 (1)	1.00	1.12	2.23	2.23	0.254	-1
3 (1)	1.12	1.12	1.12	1.12	0.254	0.0934
4 (1)	1.32	1.09	0.660	0.660	0.254	0.0133
5 (1)	1.82	0.908	0.467	0.467	0.151	-1
6 (1)	0.605	0.303	0.234	0.156	0.0757	-1
1 (2)	36.3	13.1	15.0	4.98	0.828	-1
2 (2)	2.23	1.87	1.87	1.66	0.828	0.0741
3 (2)	1.87	0.937	0.937	0.935	0.166	-1
4 (2)	0.935	0.468	0.468	0.467	0.0790	-1
5 (2)	0.467	0.279	0.279	0.279	0.117	0.0584
6 (2)	0.467	0.279	0.140	0.0930	0.0293	-1
1 (3)	30.0	11.7	13.8	21.6	0.456	1.62
2 (3)	1.87	1.67	1.67	1.87	0.456	0.539
3 (3)	0.937	0.833	0.626	0.626	0.120	-1
4 (3)	0.468	0.313	0.313	0.278	0.120	-1
5 (3)	0.279	0.179	0.166	0.166	0.0571	-1
6 (3)	0.279	0.179	0.166	0.0831	0.0286	-1
1 (4)	42.4	11.8	15.1	26.8	0.758	-1
2 (4)	1.67	1.08	0.943	0.888	0.231	-1
3 (4)	0.555	0.538	0.471	0.444	0.223	-1
4 (4)	0.278	0.179	0.157	0.148	0.0537	-1
5 (4)	0.159	0.0966	0.0966	0.0966	0.0218	0.000569
6 (4)	0.159	0.0966	0.0966	0.0483	0.0218	0.000569
1 (5)	35.5	11.6	18.7	16.0	0.955	-1
2 (5)	0.738	0.609	0.567	0.390	0.318	-1
3 (5)	0.246	0.203	0.189	0.195	0.0637	-1
4 (5)	0.123	0.0677	0.0630	0.0628	0.0191	-1
5 (5)	0.0615	0.0343	0.0340	0.0340	0.0168	-1
6 (5)	0.0615	0.0343	0.0340	0.0170	0.00421	-1

outside the fissile region including: 4 radial subdivisions, 3 azimuthal subdivisions and 2 vertical subdivisions to arrive outside the vessel. An energy group was added to the previous group structure by subdividing the highest energy group into two: above 3 MeV and from 3 to 0.5 MeV. Thus we have 49 spatial cells and 7 energy groups.

As far as the division of the fundamental mode for tallying purposes is concerned (the “global” tallies), the 9 sub-divisions shown in Fig. 23 were reduced to 5 (shown in Fig. 24) and the above vertical sub-division was maintained, making 10 global tallies.

The usual superhistory of 10 fission generations was adopted. The number of starting fission neutrons was less than in previous sample problems: starting at 20,000 and increasing to 80,000. An optimized set of space/energy cell importances already existed for a similar problem (Burn et al., 2012) (a ^{252}Cf primary start-up source in a single assembly) and was used as the starting set. As already discussed, such problems can be solved by decoupling the calculation. Therefore the exercise here, rather than to generate an optimized set of importances, was to test the feasibility of going outside the core within the eigenvalue calculation, and thus avoid the approximation (and work) of discretizing the fundamental mode and presenting the fission distribution in an appropriate form as a fixed source.

An iterative procedure was followed, the optimum importances generated at one step being employed at the next, firstly using 1 fission generation group for the importances and then passing to 5 (2-2-2-2-2). The results are given in Table 14, where “fgg” denotes the number of fission generation groups as in Table 12 and “n” denotes the number of starting neutrons of the superhistory. Presented in Table 14, as well as the $1/q_c$ values, defined in the description of Table 12, are three of the eleven responses together with their fractional standard deviations: D_1 is the ex-core response (see first paragraph in this Section), D_2 is the fission rate in the furthest East segment (see Fig. 24) and lower axial part and D_3 is the fission rate in the furthest West segment and upper axial part.

The direct estimates and function values of the second moment for this problem are in poorer agreement than for the previous problems because of the deeper penetration of the local response. However they are still within roughly a factor of 2 (as are therefore the $1/q_c$ values), which as already mentioned is good by shielding standards. Furthermore, as it is a reasonably deep penetration problem, the analog efficiency is very low and cannot be directly estimated (only the function value, $1/q_c \text{ fcn anal}$, is given).

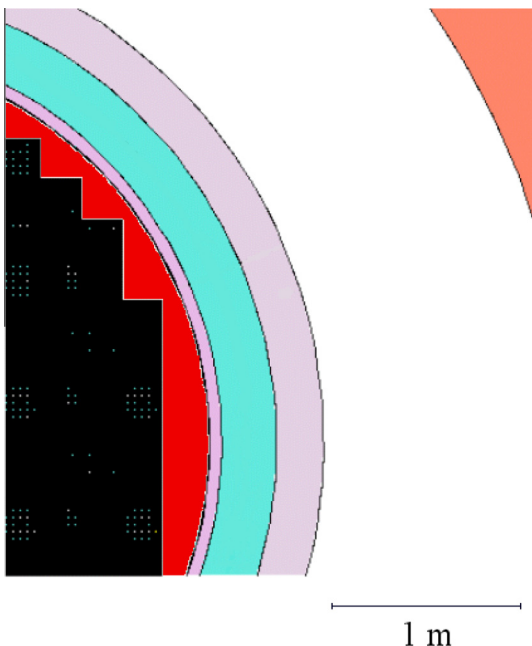


Fig. 22. PWR 3-D ex-core problem showing a horizontal section with ex-core neutron detector in the PV well.

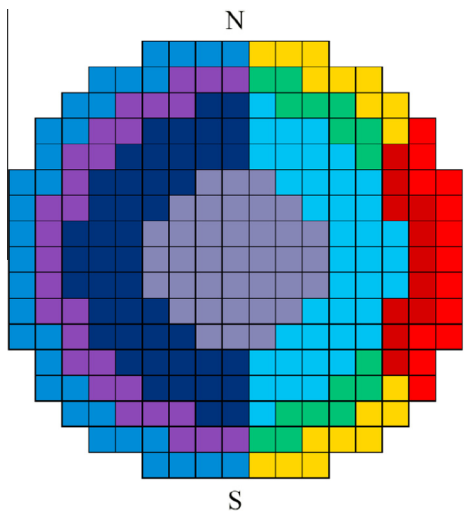


Fig. 23. PWR 3-D ex-core problem showing 9 radial subdivisions of fissile region for VR.

The responses in Table 14 are unnormalized as only the variation between steps (as well as the fsd's) is of interest. We see that the proposed technique can indeed calculate satisfactorily the ex-core response within the eigenvalue mode – the three responses presented (and eight not presented) fluctuate reasonably over the four steps and the fundamental mode looks to be maintained while the ex-core response is simultaneously calculated. The error of the local response (10–13%) is far larger than that of the components of the fundamental mode (2–5%), as expected. (Note that although the fsd's at step 4 are worse than at step 3, the time is much less – because of less splitting and more RR – so the efficiency is greater.)

The gain of the final importances over the starting set ($0.571/0.133 = 4.29$) is not large but as already underlined that is not the point of the exercise for this problem. Also the gain in going from 1 to 5 fission generation groups for the importances dependence

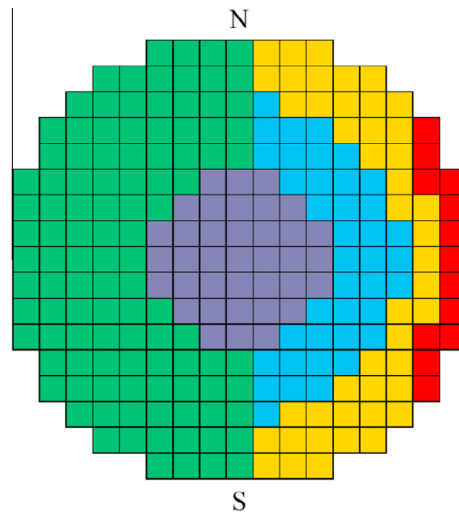


Fig. 24. PWR 3-D ex-core problem showing 5 radial subdivisions of fissile region for "global" tallying.

is much less than 2 ($0.571/0.548 = 1.04$). This is expected as it is well known that it is fissions in the outermost assemblies (and indeed in their outer pins) that predominate for core leakage. Thus transport between fissions within the core should not be important. Possibly superhistories of more than one fission generation might therefore not be helpful. However the multi-response feature – optimizing to the local response and to components of the fundamental mode simultaneously – is crucial.

As the fsd's on the local ex-core detector results in Table 14 are relatively large (10–15%), the problem was further examined by running 30 independent calculations (each starting with a different random number seed). These calculations employed the "optimum" importances at step 4 and ran a single superhistory of 10 fission generations (as in Table 14). The results are shown in Table 15. We see, as expected, lower fsd's and a fom_c (0.635) that is consistent with the direct estimate of $1/q_c$ with the same importances in the last row of Table 14 (0.571). Thus the results with relatively high errors in Table 14 are supported by the more accurate results in Table 15.

6.4.1. Verifying that the fundamental mode is maintained

It is of interest to carry out the same analysis on this problem as was made on the PWR-3D problems of Section 6.2, to check that the fundamental mode is not skewed by the forcing of the neutrons out of the fissile region in one direction. Thus the same analysis as that leading to Figs. 17 and 18 in Section 6.2.4 was made with the same Shannon entropy mesh, 1000 superhistories each of 10 fission generations and 500,000 starting neutrons for each superhistory and with the optimum importances from step 4 in Tables 14 and 15.

Note that the geometrical model of Problem 6.4 was identical to those of Problems 6.2. Therefore the analog-analog results in Figs. 16–18 were valid. However in the tracking the random number sequence diverged due to a different cell sub-division for VR. Therefore it was of interest to compare the analog–analog results generated on this problem with those in Figs. 16–18. The results are shown in Fig. 25 (where all non-zero stochastic results are shown). Thus we have a very rough idea of the uncertainty in these verifications of the fundamental mode.

In Fig. 26, the analog–analog results are compared with the DSA-optimized results (all non-zero stochastic results are shown). Comparing Fig. 26 with Figs. 17 and 18, we infer that the

Table 14

Comparison of direct estimates and function values of $1/q_c$ for PWR 3-D ex-core problem.

Step	$n/1000$	fgg run	fgg opt.	D_1 (fsd)	D_2 (fsd)	D_3 (fsd)	$1/q_c$ est	$1/q_c$ fcn anal	$1/q_c$ fcn run = B	$1/q_c$ fcn opt = A	A/B
1	20	1	1	1.065 (0.1403)	30.1 (0.0674)	128.0 (0.0360)	0.133	4.4E-6	0.317	1.31	4.13
2	40	1	1	1.126 (0.0995)	29.1 (0.0446)	128.4 (0.0313)	0.629	3.8E-6	1.12	1.30	1.16
3	80	1	5	1.187 (0.1036)	28.1 (0.0297)	124.6 (0.0234)	0.548	3.5E-6	1.25	1.72	1.38
4	80	5	—	1.422 (0.1328)	27.9 (0.0338)	134.8 (0.0271)	0.571				

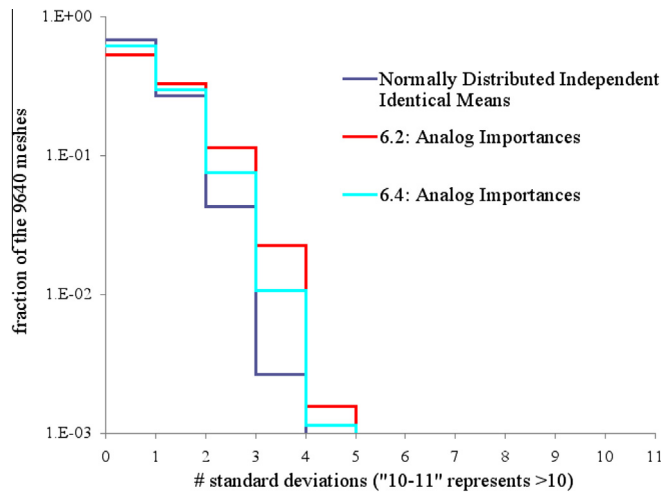


Fig. 25. Measure of the maintenance of the fundamental mode: comparison of analog-analog results of problems 6.2 with analog-analog results of problem 6.4.

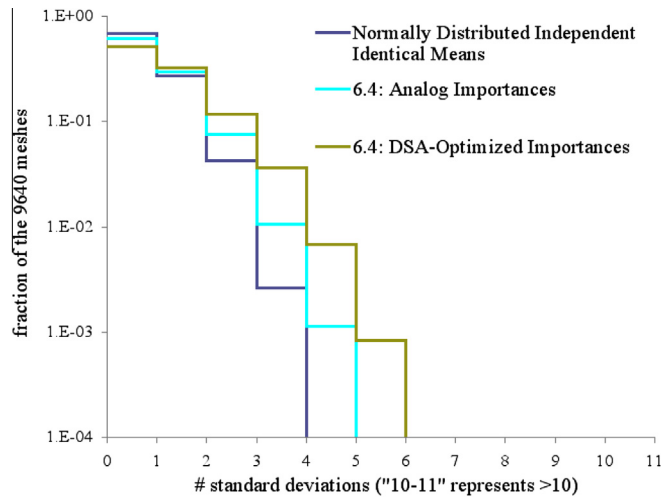


Fig. 26. PWR 3-D ex-core problem: measure of the maintenance of the fundamental mode; analog-analog, analog-optimum importances.

Table 15

Results of selected responses and fom_c for 30 independent calculations with final importances for PWR 3-D ex-core problem.

Step	n	fgg run	D_1 (fsd)	D_2 (fsd)	D_3 (fsd)	fom_c
4	$80,000 \times 30$	5	1.205 (0.0230)	28.5 (0.0064)	130.1 (0.0034)	0.635

calculation of an ex-core local response does not distort the fundamental mode.

7. Conclusions and discussion

The DSA multi-response capability has been modified to work within a source-iteration eigenvalue calculation, improving the statistics of a local detector whilst maintaining the fundamental mode. Indeed, in some cases it looks as if it is the only way of obtaining a small local response (without of course decoupling the calculation in some way). The DSA functions provide values that are in good agreement with the direct estimates. Thus the gains in efficiency are quite well predicted and one assumes that the optima are true.

The method has been tested on local responses that are both in- and ex-core. In both cases the results were satisfactory. Although in the ex-core test problem the local detector was not too far from the core, the optimum was reached easily which suggested that it might be feasible to calculate local detectors still further out from the core. This was a surprise.

Allowing a number of fission generations between normalizations of the fission source (i.e. superhistories) may help in maintaining the fundamental mode and also very probably allows a greater skewing of the track population to calculate a local in-core detector, compared with a single fission generation. However if VR parameters are employed that are independent of the fission generations, variance is introduced between fission generations. The solution adopted was to allow the VR parameters to vary according to the fission generation (or group of fission generations). As well as reducing the above variance by softening the Russian roulette between generations, it was expected that this would allow the neutron population to be fitted better to the local detector at later fission generations within the superhistory. It turned out that allowing such dependence of the VR parameters on the fission generation yielded an increase in efficiency of approximately a factor of 2 when the local detector was in-core. This factor looked surprisingly problem-independent. Instead it was much less than 2 for the ex-core detector, which was expected because in the ex-core case, transport between fission sites counts little (because fission in the external pins of the outer assemblies gives the main contribution).

For one of the in-core problems, a comparison was made with the “classic” formalism based purely on the adjoint flux and employing the estimated responses to normalize the individual adjoint functions. The results deteriorated by an order of magnitude. No explanation was forthcoming for this difference between the two techniques.

No weight dependence has been tested here. For an in-core detector, the author can only imagine a weight dependence being employed together with the exponential transform, which itself might be employed only if the detector is extremely small. Instead, biasing the fission source toward higher energies is a technique that is often employed with an ex-core detector and would be interesting to test.

We return to the question of biases raised in Section 2. As discussed in Brissenden and Garlick (1986), biases in the response estimates (and sometimes in their error estimates) are an intrinsic part of the source-iteration Monte Carlo algorithm. Thus as the approach proposed here employs the source-iteration Monte Carlo

algorithm, there is no purpose in attempting to prove unbiasedness. However, there are some outstanding issues:

Firstly it has been shown (Brown, 2010) that biases in differential responses are generally greater than those in k_{eff} and the local responses considered here are very differential. (It has also been shown (Brissenden and Garlick, 1986; Brown, 2010) that biases in response estimates are proportional to the inverse of the number of neutrons per cycle and thus reduce as the cycle size increases.) Such biases have not been quantified here, but employing superhistories reduces the number of normalizations and thus reduces these biases as well as the variance bias (present when statistics are made between normalization generations) (Brissenden and Garlick, 1986).

Secondly as the approach presented here of necessity strongly distorts the distribution of tracks, the question exists whether such distortion of the track numbers transmits through to the expected distribution, i.e. to the fundamental mode. Verifications of this have been made in Sections 6.2.4 and 6.4.1 and, whilst as expected the fundamental mode with VR is noisier than that without VR, the evidence presented for these realistic problems indicates that it does not look to be distorted (with respect to the distribution without VR). This does not of course constitute any kind of proof, which would require a much greater calculational effort.

Finally there is what may be termed the second-order issue of the impact of a noisier fundamental mode distribution (brought about by VR) on the bias in the response estimates. This has not been investigated.

Acknowledgments

The author would like to thank Reg Brissenden for introducing him to the world of Monte Carlo in the eigenvalue source iteration scheme (nearly 30 years ago). More recently Art Forster impressed on the author the fact that in realistic LWR calculations (and not only), it is necessary to run an appreciable number of fission cycles, however large the fission source can feasibly be made, so as to cover the fundamental mode.

The PWR-2D problem formed part of a wider collaboration with Giovanni Bruna and Antonio Sargeni of IRSN concerning the problem of flux tilt.

The author would like to take this opportunity to thank Salvatore Podda and Pietro D'Angelo of the Informatics Dept., ENEA Frascati for support in the implementation and running of MCNP on the sp5 (AIX) machines at ENEA, Frascati.

The author also wishes to express his appreciation of the efforts of the referees whose various suggestions improved the manuscript. In particular the effort to demonstrate when the fundamental mode is, and is not, maintained (Figs. 16–18 and 26) and the generation of less noisy results for problem 6.4 (Table 15) is due to one of the referees.

This work has been funded under the program agreement: Italian Ministry of Economic Development – ENEA, “Annual Plan 2012, Project B.3.1: Development of Expertise in Nuclear Safety”.

References

Becker, T.L., Wollaber, A.B., Larsen, E.W., 2007. A hybrid Monte Carlo – deterministic method for global particle transport calculations. *Nucl. Sci. Eng.* 155, 155–167.

- Booth, T.E., 1992. Monte Carlo variance reduction approaches for non-Boltzmann tallies. Los Alamos National Laboratory, LA-12433.
- Booth, T.E., Burn, K.W., 1993. Some sample problem comparisons between the DSA cell model and the Quasi-deterministic method. *Ann. Nucl. Energy* 20 (11), 733–765.
- Booth, T.E., 2002. Pulse-height tally variance reduction in MCNP. Los Alamos National Laboratory, LA-13955.
- Booth, T.E., 2006. Genesis of the weight window and the weight window generator in MCNP – a personal history. Los Alamos National Laboratory, LA-UR-06-5807.
- Booth, T.E., 2012. Common misconceptions in Monte Carlo particle transport. *Appl. Radiat. Isot.* 70, 1042–1051.
- Brissenden, R.J., Garlick, A.R., 1986. Biases in the estimation of k_{eff} and its error by Monte Carlo methods. *Ann. Nucl. Energy* 13 (2), 63–83.
- Brown, F.B., Kiedrowski, B., Martin, W., Yesilyurt, G., 2009. Advances in Monte Carlo criticality methods. Los Alamos National Laboratory, LA-UR-09-02442.
- Brown, F.B., 2010. Reactor physics calculations with MCNP. In: *Reactor Physics Analysis with Monte Carlo*. Los Alamos National Laboratory, LA-UR-10-02762.
- Burn, K.W., 1990. Extension of the Direct Statistical Approach to a volume parameter model (non-integer splitting). *Ann. Nucl. Energy* 17 (6), 293–316.
- Burn, K.W., 1992. Complete optimization of space/energy cell importances with the DSA cell importance model. *Ann. Nucl. Energy* 19 (2), 65–98.
- Burn, K.W., 1995. Extending the Direct Statistical Approach to include particle bifurcation between the splitting surfaces. *Nucl. Sci. Eng.* 119, 44–79.
- Burn, K.W., 1996. Learning aspects of the Direct Statistical Approach to the optimization of Monte Carlo radiation transport calculations. In: *Workshop on Adaptive Monte Carlo Methods*, Los Alamos, NM.
- Burn, K.W., 1997. A new weight-dependent DSA model. *Nucl. Sci. Eng.* 125, 128–170.
- Burn, K.W., Nava, E., 1997. Optimization of variance reduction parameters in Monte Carlo radiation transport calculations to a number of responses of interest. In: *Proc. Int. Conf. Nuclear Data for Science and Technology*. Trieste, Italy, pp. 260–264.
- Burn, K.W., Gualdrini, G., Nava, E., 2000. Variance reduction with multiple responses. In: *Proc. MC 2000*. Lisbon, Springer, pp. 687–695.
- Burn, K.W., Gualdrini, G., 2002. Optimizing the Monte Carlo evaluation of neutron spectra within a thermal neutron calibration facility, ENEA, RT/2002/54/ION.
- Burn, K.W., Casalini, L., Nava, E., Petrovich, C., Tecchio, L., 2005. Shielding calculations for a 100 MeV 30 mA proton beam. *Rad. Prot. Dosimetry* 116 (1–4), 89–94.
- Burn, K.W., 2011. Optimizing Monte Carlo to multiple responses: the Direct Statistical Approach, 10 years on. *Nucl. Technol.* 175, 138–145.
- Burn, K.W., Bruna, G., Normand, B., 2012. Impact of the heavy steel reflector of a current large PWR design on some safety features. In: *Proc. of TopSafe, Safety in Reactor Operations*, Helsinki.
- Cinotti, L., Locatelli, G., Abderrahim, H.A., Monti, S., Benamati, G., Tucek, K., Struwe, D., Orden, A., Corsini, G., Le Carpenter, D., 2008. The ELSY project. In: *Proc. of PHYSOR 2008*. Interlaken, Switzerland.
- Dubi, A., Elperin, T., Dudziak, D., 1982. Geometrical splitting in Monte Carlo. *Nucl. Sci. Eng.* 80, 139–161.
- Dubi, A., 1985. General statistical model for geometrical splitting in Monte Carlo – parts I and II. *Transp. Theory Stat. Phys.* 14 (2), 167–193, and 195–221.
- Ivanov, K., Avramova, M., Kamerow, S., Kodeli, I., Sartori, E., 2011. Benchmark for uncertainty analysis in modeling (UAM) for design, operation and safety analysis of LWR's: volume I: Specification and support data for the neutronics cases (phase I). OECD Nuclear Energy Agency, NEA/NSC/DOC(2011).
- Jinaphanh, A., 2012. Studies concerning the convergence of Monte Carlo criticality calculations: employment of a deterministic calculation and automatic detection of the transient. Ph.D. thesis in Applied Physics. University of Grenoble (in French).
- Solomon, C.J., Sood, A., Booth, T.E., 2009. A weighted adjoint source for weight-window generation by means of a linear tally combination. In: *Proc. Int. Conf. Advances in Mathematics, Computational Methods, and Reactor Physics*. Saratoga Springs, NY (3–7 May).
- Van Wijk, A.J., Van den Eynde, G., Hoogenboom, J.E., 2011. An easy to implement global variance reduction procedure for MCNP. *Ann. Nucl. Energy* 38, 2496–2503.
- Wagner, J.C., Blakeman, E.D., Peplow, D.E., 2007. Forward-weighted CADIS method for global variance reduction. *Trans. Am. Nucl. Soc.* 97, 630–633.
- X-5 Monte Carlo Team, 2005. MCNP – A general Monte Carlo n-particle transport code, version 5, Los Alamos National Laboratory, vol. I: Overview and theory, LA-UR-03-1987; vol. II: User's guide, LA-CP-03-0245; vol. III: Developer's guide, LA-CP-03-0284.